As originally published in the SMTA Proceedings.

The Effect of Thermal Cycling Profile on Thermal Fatigue Performance of an 84-Pin Thin Core BGA with Hybrid, Homogeneous, and Resin Reinforced Low Temperature Solder Interconnects

Dan Burkholder[1], Raiyo Aspandiar[2], Yunfei Wang[2], Russ Brown[3], Richard Coyle[4], Babak Arfaei[5], Vasu Vasudevan[6], Aileen Allen[7], Keith Howell[8], Qin Chen[9], Derek Daily[10], Haley Fu[11], Carol Handwerker[12], Ralph Lauwaert[13], Daniel Werkhoven[13], Kei Murayama[14], Hongwen Zhang[15], Francis Mutuku[15], Huaguang Wang[15], Morgana Ribas[16], and Murali Sarangapani[17]

[1]Intel Corporation, Chandler, AZ, USA, [2]Intel Corporation, Hillsboro, OR, USA, [3]Intel Corporation, Folsom, CA, USA, [4]Nokia, Murray Hill, NJ, USA, [5]Binghamton University, Binghamton, NY, USA, [6]Dell Technologies, Round Rock, TX, USA, [7]HP, Inc., Palo Alto, CA, USA, [8]Nihon Superior Co., Ltd., Osaka, Japan, [9]Eunow, Suzhou, China, [10]Senju Comtek Corp, Santa Clara, CA, [11]iNEMI, Shanghai, China, [12]Purdue University, West Lafayette, IN, USA, [13]Interflux Electronics NV, Belgium, [14]Shinko Electric Industries Co. LTD., Nagano, Japan, [15]Indium Corporation, Clinton, NY, USA, [16]MacDermid Alpha Electronics Solutions, Bengaluru, India, [17]Heraeus Materials Singapore Pte Ltd, Singapore

dan.s.burkholder@intel.com raiyo.f.aspandiar@intel.com

ABSTRACT

There is an increasing interest in many market segments to use solder alloys with lower melting temperatures for electronics assembly. Low temperature solders can provide manufacturing, economic, and environmental benefits. Since 2015, the International Electronics Manufacturing Initiative (iNEMI) Low Temperature Solder Process and Reliability (LTSPR) Project has been evaluating Low Temperature Solder (LTS) paste formulations based on the Bi-Sn system. This paper summarizes the findings from a thermal cycling test to evaluate the effect of thermal cycling profile on thermal fatigue performance of low temperature solders.

The study uses a daisy chained printed circuit board and two daisy chained ball grid array (BGA) test vehicles, a 192-pin chip array BGA (CABGA192) and an 84-pin thin core BGA (CTBGA84). The test matrix includes multiple LTS solder alloys designated by code names. The alloys are down selected from the larger project alloy matrix based on assembly effectiveness and mechanical test performance. There are two types of solder alloys, so-called ductile metallurgies that employ alloy modifications to improve the properties of the basic Bi-Sn alloy, and joint reinforced pastes (JRP) that employ resin additions that generate in situ fillets during reflow to provide joint support. Components manufactured with the established SAC305 (Sn3.0Ag0.5Cu) composition are used as the baseline for the study.

Three types of LTS solder joints are evaluated, homogeneous, hybrid (heterogeneous), and hybrid formed with joint reinforced pastes (JRP). Hybrid joints have a SAC BGA soldered with a ductile metallurgy LTS solder paste. The resultant solder joint consists of an unmelted SAC region at the package side of the joint and a melted region at the PCB side containing Bi from the solder paste. A hybrid joint also may be described as heterogeneous because it contains two regions with clearly distinct microstructures, compositions, and properties. Homogeneous joints are created when a BGA manufactured with LTS solder spheres is soldered to the PCB using a LTS solder paste with matching composition. A JRP joint is a special type of hybrid joint that has resin fillets that form during reflow to enhance joint support.

To address the resources required for a comprehensive evaluation of low temperature solder technology, the International Electronic Manufacturing Initiative (iNEMI) launched the BiSn-based Low Temperature Soldering Process and Reliability (LTSPR) Project in 2015. Now in this third iNEMI LTSPR phase, testing is conducted with two distinct Accelerated Temperature Cycling (ATC) profiles, 0/100° C (IPC-9701B, TC1) and -15/85° C (selected due to homologous temperature considerations between Sn-Ag-Cu and Bi-Sn solder and maintaining a similar delta T [100° C] across both ATC profiles). This interim paper reports the thermal cycling results for the 84-pin thin core BGA component (CTBGA84) tested with the -15/85° C profile and compares these results (as a companion paper) to the CTBGA84 tested with the 0/100° C profile, presented in a previous publication [61]. Weibull statistics, microstructural characterization, and failure mode analysis are used to compare the differences in alloy performance and to compare the performance of hybrid and homogeneous solder joint configurations.

At the time of writing this paper, two of the seven -15/85 °C profile legs had not yet reached the N63 failure criteria per IPC-9701B (homogeneous Sultan 2 at 19% failure rate with 25,000 cycles run and hybrid Beserah JRP at 58% failure rate with 28,500 cycles run). However, as many cycles have already been completed for this experiment and the Weibull slope (β) and Correlation Coefficient (r^2) for these two legs are healthy, only a relatively small change in the final Weibull statistics are expected once N63 is reached. The Weibull statistics data will be updated again when this experiment finishes completely.

Key words: Low temperature solder, thermal fatigue reliability, thermal cycling, accelerated temperature cycling, hybrid solder joints, homogeneous solder joints, joint reinforced solder pastes, resin, bismuth, solder ball drift.

INTRODUCTION

Low Temperature Solder

The development and implementation of Low Temperature Solders (LTS) for electronic assembly is being driven by technical, economic, and environmental requirements. A notable motivation for implementing low temperature solder processes is to minimize dynamic warpage (flatness as a function of temperature) of ball grid array (BGA) components and printed circuit boards. Warpage during solder reflow can reduce assembly yields and result in unpredictable early field failures by creating defects such as head on pillow (HoP), Non-Wet Open (NWO), and solder ball bridging (SBB) [1]. Aspandiar et al. [2] and Mokler et al. [3] have presented data that suggest component warpage could be minimized if reflow is performed in the range of 160 to 180 °C. This temperature range is well-below the current Sn-Ag-Cu (SAC) reflow range of 240-260 °C. The Mokler study shows a 30-50 % reduction in warpage in a flip chip BGA (FCBGA) when reflowed below 180 °C. However, replacing the current SAC alloys with low temperature solders requires characterizing thermal fatigue performance of low temperature solders to ensure they meet reliability performance expectations. Additionally, assembly processes may need to be created or adapted to support implementation of these alloys.

Low temperature soldering, in the context of these current industry discussions, refers to reflow at a peak temperature below 200 °C. The leading solder alloy candidates for reflow below 200 ºC are based on the Bi-Sn binary alloy system that has a melting point of 138 ºC at its eutectic composition of approximately 42 wt.% Sn and 58 wt.% Bi [4]. The metallurgy and technology of low temperature solder alloys is evolving rapidly and detailed information on solder assembly processing, alloy development, and reliability testing can be found in several comprehensive reviews [5-10]. The 42Sn-58Bi binary eutectic alloy initially was considered a viable Pb-free candidate to replace Sn-Pb solder, so there are already many available reports on its performance [11-15]. However, independent investigations confirmed the poor mechanical shock resistance [16] and lower fatigue life [14] of 42Sn-58Bi, which was attributed to its brittle two-phase lamellar microstructure.

Since those earlier evaluations of the 42Sn-58Bi binary eutectic alloy, solder suppliers have developed new low temperature solder pastes to improve the reliability limitations of the binary 42Sn-58Bi alloy. For example, the ductility of the Bi-Sn alloy can be enhanced by incorporating elemental additions that promote grain refinement, precipitate hardening or solid solution strengthening [3]. In this way, the Bi-Sn microstructure is modified to combine its inherent mechanical strength with better ductility and fatigue resistance to withstand mechanical stresses due to shock or cyclic stresses, such as those associated with mechanical shock or thermal cycling, respectively. LTS alloys with enhanced properties due to elemental additions often are referred to as ductile metallurgies. Another option is the reinforcement of the solder joint by incorporating resin in the solder paste. In this case, the resins contained in the solder paste cure during the reflow, forming a physical reinforcement layer that acts as a mechanical barrier around the metallic solder joint [17]. LTS alloys with enhanced properties due to resin additions are referred to as joint reinforced pastes (JRP).

The primary focus of recent industry LTS studies is on the assembly and reliability challenges of hybrid (also called heterogeneous, or mixed metallurgy) ball grid array (BGA) solder joints. A hybrid LTS solder joint is defined as a SAC BGA that is reflow assembled with LTS solder paste. LTS hybrid BGA solder joints consist of an upper region of unmelted SAC solder and a lower region of melted SAC solder mixed with the Bi-Sn solder paste. Figure 1 shows a back scattered electron (BSE) image of a hybrid solder joint. The Bi presents as the bright white phase in the backscattered imaging mode. Independent evaluations of Bi-Sn solders with ductile alloying or resin reinforcement have demonstrated promising results resisting mechanical shock [3, 18, 19] and thermal fatigue [20] in hybrid SAC-BiSn BGA assemblies.

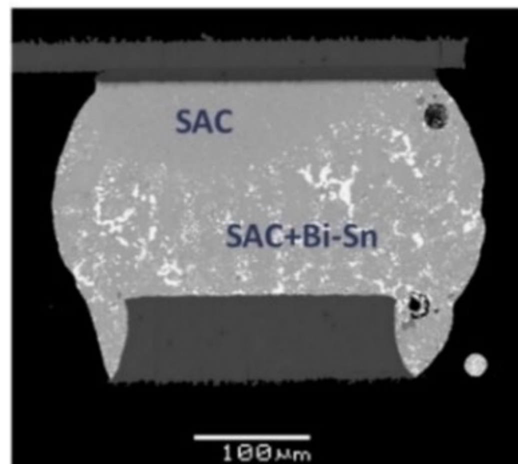

Figure 1. A cross-sectional back scattered scanning electron image of a hybrid or heterogenous ball grid array solder joint (figure published previously [37]).

The initial applications for low temperature solder have been in portable consumer electronics such as laptop computers [21], thus most of the hybrid reliability testing has been focused on mechanical shock and drop requirements [18, 19, 22-27]. However, some applications also require acceptable thermal fatigue reliability, and there are much fewer thermal cycling studies compared to drop/shock studies. Existing data are limited in scope, mostly due to the large number of variables under consideration such as solder processing parameters, alloy compositions, paste formulations, and component type [1, 9, 20, 23, 28, 29]. Despite more recent thermal cycling activity [30-34], many gaps remain in thermal fatigue data for hybrid solder joints.

To address the resources required for an unbiased and comprehensive evaluation of low temperature solder technology, the International Electronic Manufacturing Initiative (iNEMI) launched the BiSn-based Low Temperature Soldering Process and Reliability (LTSPR) Project in 2015. The project is supported by multiple stakeholders, including a diverse mix of Original Design Manufacturers (ODMs), Original Equipment Manufacturers (OEMs), Electronic Manufacturing Services (EMS), material suppliers, and universities. The first two phases of the project explored material selection, development, and optimization of surface mount processes specific to low temperature solders, and evaluation of mechanical shock performance [22, 24, 26, 27, 35, 36]. The project is currently in its third phase, which is evaluation of thermal cycling performance.

The iNEMI LTSPR thermal cycling test matrix includes multiple LTS solder alloys that were down selected from the first two phases based on assembly effectiveness and mechanical test performance. These alloys include the ductile metallurgies that employ alloy modifications to improve the properties of the basic Bi-Sn alloy, and joint reinforced pastes (JRP) that employ resin additions that generate in situ fillets during reflow to provide joint support. Components manufactured with the established SAC305 (Sn3.0Ag0.5Cu) composition are used as the control for the study.

EXPERIMENTAL

Test Vehicle

Component and Test Board Description

The test vehicle components and test board information for this experiment can be found in a prior publication [62]. Appendix A, Table A-1, contains the attributes of the BGA package and PCB [37] used in this experiment. Appendix A, Figure A-1, contains the CABGA192 and CTBGA84 daisy chained components and pin diagrams with die sizes and locations [37, 39]. Appendix A, Figure A-2, contains a fully populated, daisy chained PCB and the daisy chained CABGA192 and CTBGA84 components [37].

Board Assembly Parameters

Experimental Design

The experimental design information for this experiment can be found in a prior publication [62]. Appendix B, Table B-1, contains the 7 experimental legs for these temperature cycling tests [37].

Stencil Design and Printed Solder Paste Volume

The stencil design and printed solder paste volume information for this experiment can be found in a prior publication [62]. Appendix C, Figure C-1, contains the stencil aperture designs for the two components (CABGA192 and CTBGA84) on the Alloy ATC TV board [37]. Appendix C, Figure C-2, contains the variability chart for the printed solder paste transfer efficiency for the solder pastes used in this study to assemble the Alloy ATC TV board [37, 61, 62].

Reflow Soldering Profiles

The reflow soldering profiles information for this experiment can be found in a prior publication [62]. Appendix D, Table D-1, contains the Bi weight%, Ag weight%, initial melting and liquidus temperatures of the five solder pastes used in this study [37]. Appendix D, Figure D-1, contains the peak reflow temperature (PRT) and Time Above Liquidus (TAL) information for the alloys used in this study [37]. Appendix D, Figure D-2, contains the thermocouple locations used on the Alloy ATC TV board. Appendix D, Figures D-3, D-4, D-5, D-6, D-7, D-8 and D-9 [37, 61, 62], contain the reflow profiles for all 7 experimental legs.

Post Reflow Soldering Daisy Chain Resistances

The post reflow soldering daisy chain resistance information for this experiment can be found in a prior publication [62]. Appendix E, Figure E-1, Resistances of the Daisy Chains for the two Component Types on the Alloy ATC TV boards after reflow soldering for 16 components of each type on each board after they were reflow soldered [37, 61, 62]. Some daisy chain resistance values for the CTBGA84 in the hybrid Golden Pillow 2 leg are outliers (as denoted by the red square data points in Figure E-1). Figure 2 shows 3D Computer Tomography (CT) X-ray images and scanning electron microscopy images, in the backscattered electron (BSE) mode of joints, with an appearance like that of a Head-on-Pillow (HoP) solder defect, in the hybrid Golden Pillow 2 JRP leg for the CTBGA84 component [37, 61].

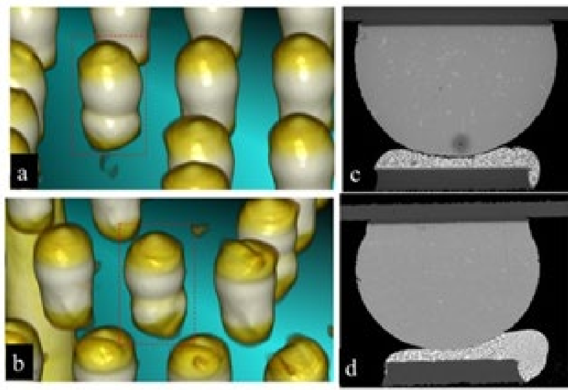

Figure 2. Examples of HoP-like solder joints in the hybrid Golden Pillow 2 JRP leg of CTBGA84 components (figures published previously [37, 61]).

Similar solder joint structures were reported in the Process development phase of the current iNEMI LTSPR project [22]. These defects are believed to form by the premature gelling of the resin in the JRP paste before the solder has become molten and has wet the BGA SAC sphere. This issue was mostly seen with the finer pitch CTBGA84 component. Increasing the initial reflow ramp rate to >3°C/sec (from 1-2°C/sec) for the hybrid Golden Pillow 2 leg is one suggested method to eliminate these defects [22], but this was difficult to achieve on the ATV test board.

Microstructural Characterization and Failure Analysis

Baseline characterizations were performed on representative board level assemblies from each of the test cells to document the solder joint quality and basic solder microstructure at time zero, before the start of temperature cycling. This enabled comparisons to be made between samples at time zero to samples that were removed subsequently from the temperature cycling chamber (after sample electrical failure had occurred, opportunistically, at different cycle read points during the test) for characterization and failure mode analysis.

Microstructural characterizations and failure mode analyses were done using metallographic cross-sectioning and using the Scanning Electron Microscope (SEM) operating in Backscattered Electron (BSE) imaging mode. With BSE imaging, the number of electrons reaching the detector is proportional to the atomic number (*Z*), which makes it effective for differentiating phases. This has been demonstrated for SAC microstructures [41-43] and is particularly useful for differentiating the high-*Z* Bi phase in solder microstructures [26, 41, 43]. The SEM operating in the secondary electron imaging (SEI) mode was used to observe the resin fillets.

Accelerated Temperature Cycling

Accelerated temperature cycling (ATC), or thermal cycling (TC), is the recognized technique for evaluating the thermal fatigue performance of solder attachments. Daisy chained components and circuit boards enable electrical continuity testing after surface mount assembly and in situ, continuous monitoring during thermal cycling. The thermal cycling plan includes two distinct thermal cycling profiles, 0/100 °C and -15/85 °C. The 0/100 °C profile is designated as TC1 in the IPC-9701B performance document that provides guidance for assessing reliability of surface mount attachments [44]. Both ATC profiles used in this study had a nominal hot and cold ramp and dwell times of 10 minutes, resulting in a total cycle time of 40-minutes.

The -15/85 °C profile is not part of the IPC-9701B standard, but there was a particular reason for using this thermal cycling profile, a reason directly related to the lower melting temperature of the Bi-Sn solder.

The homologous temperature, T_h is defined as the ratio of the temperature a material is at, T, and its melting point, T_m, with the calculation done on the Kelvin scale; $T_h = T(K)/T_m(K)$. Material degradation processes, such as creep that occurs when subjected to fatigue stresses, as well as annealing processes, such as recrystallization and grain growth of the microstructure within metals, occur at T_h greater than 0.4 [45]. At temperatures where T_h is greater than 0.9, the strength and hardness of metals reduces precipitously. This thermal cycling profile was used mainly due to the concern that the upper dwell temperature of 100 °C in the original temperature cycling profile (0/100 °C) was above a homologous temperature of 0.9 for BiSn solders.

Figure 3 displays the homologous temperature (T_h) comparison between Sn-Ag-Cu solder and Bi-Sn solder. Since Bi-Sn solder has a lower melting point (~138 °C) than Sn-Ag-Cu solder (~217 °C), its homologous temperature line is above that of Sn-Ag-Cu. At the upper dwell temperature of 100 °C for the 0/100 °C thermal cycling test, T_h for Bi-Sn solder is 0.92. To lower the T_h below 0.90, 85 °C was chosen as the upper dwell temperature for an alternate thermal cycling profile. The T_h for Bi-Sn solder at 85 °C is 0.87. The T_h for SAC is 0.73 at 85 °C.

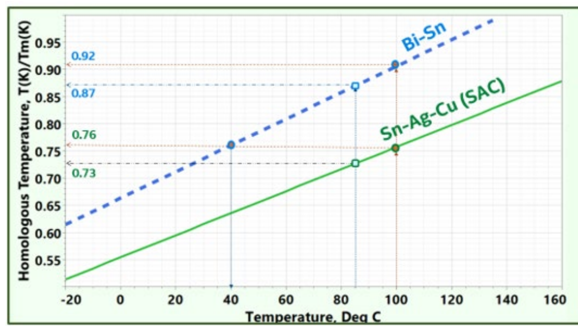

Figure 3: Homologous Temperature (T_h) Comparison between Sn-Ag-Cu solder and Bi-Sn solder [45].

The difference between the two thermal cycling dwell temperature extremes (ΔT) is a critical parameter when selecting thermal cycling test profile since in the literature, many acceleration models that have been widely used to predict the lifetimes of solder joints of electronic packages include ΔT as a key factor [46-49]. Hence, the same 100 °C ΔT was set for the second thermal cycling profile to match the original 0/100 °C profile. Consequently, the dwell temperature extremes for this second profile were set at -15 °C to 85 °C.

Nonetheless, since the paramount goal in this work was to compare the temperature cycling fatigue resistance of SAC and Bi-Sn BGA solder joints, setting the upper dwell temperature of the second thermal cycling profile at the same T_h of that for SAC at 100 °C would have been most appropriate. However, from Figure 3 it is apparent that this would require the upper dwell temperature to be at 40 °C. Using a -40 to 40 °C temperature profile would be impractical since the time needed to get adequate solder joint failures would extend beyond 3 to 5 years.

During thermal cycling, the solder joints are monitored using an event detector set at a resistance limit of ≥1000 ohms. Failure data are reported as characteristic lifetime η (the number of cycles to achieve 63.2% failure), Weibull slope β, Correlation Coefficient r^2, and 1% Cumulative Failure from a two-parameter (2-P) Weibull analysis.

RESULTS AND DISCUSSION

Solder Joint Characterization

During the reflow assembly process, the SnBi-based solder paste melts and wets the SAC balls and Cu metallization on the PCB pads. Sn and Cu dissolve into the melt until it reaches equilibrium. The microstructure and Bi distribution of hybrid joints after SMT reflow depend on variables such as reflow peak temperature, initial solder paste to solder ball volume ratio, cooling rate, and solder composition [55, 56]. Figure 4 shows low magnification BSE and SEI images of as assembled CTBGA84 samples. JRP assemblies are shown in Figure 4a through Figure 4d, and hybrid assemblies are shown in Figure 4e and Figure 4f [61]. As discussed in the assembly section, the stencil aperture was designed to produce an initial solder-paste volume-to-BGA ball volume (PBV) ratio of between 0.5 and 0.6 for all four hybrid assemblies.

Despite a constant volume ratio, there is a noticeable variation in the amount of Bi mixing in the solder joints imaged in Figure 4. This variation in Bi mixing could result from different peak reflow temperatures and time above liquidus (Appendix, Figure D-1), different flux chemistries, as well as compositional differences in Bi content and minor alloy additions of the pastes.

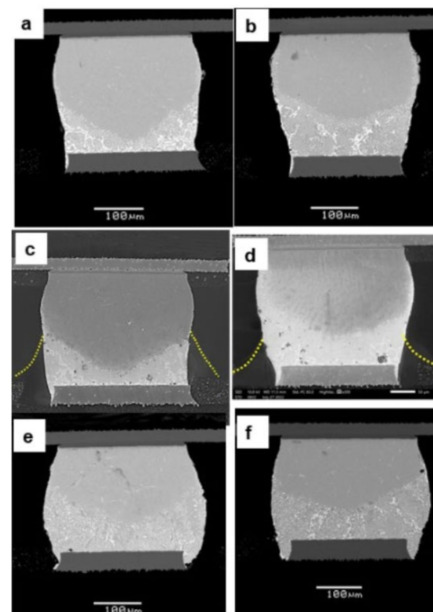

Figure 4. Cross sectional images of as-assembled hybrid and JRP CTBGA84 LTS solder joints before thermal cycling. Bismuth mixing is revealed using BSE imaging in a) Beserah JRP and b) Golden Pillow 2 JRP. Resin fillet formation is outlined in the SEI images in c) Beserah JRP and d) Golden Pillow 2 JRP. Bismuth mixing is revealed using BSE imaging in e) hybrid Red Flesh and f) hybrid Sultan 2 (figures published previously [61]).

The amount of Bi mixing was estimated using ImageJ, a public domain Java image processing program available from the National Institute of Health (NIH)) [52]. Sixteen solder joints for each leg were imaged using the SEM and the back scattered detector. The area of Bi mixed region was measured with respect to the area of entire joint. Figure 5 shows the average values of Bi mixing for the four hybrid experimental legs. For the CTBGA84 hybrid solder joints, hybrid Beserah JRP has the lowest average Bi mixing and hybrid Sultan 2 has the highest average Bi mixing.

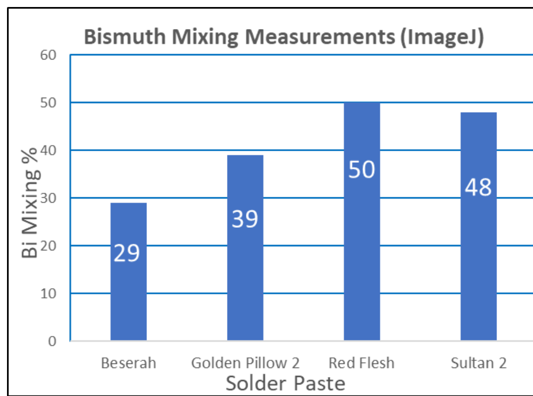

Figure 5. A bar chart of the average solder joint Bi mixing levels in the four hybrid legs for the CTBGA84 component. Bismuth mixing was estimated using the ImageJ processing program (figure published previously [61]).

Figure 6 shows the solder joint microstructures of as-assembled CTBGA84 homogeneous Red Flesh (Figure 6a) and homogeneous Sultan 2 (Figure 6b) samples before thermal cycling [61]. One key difference between Red Flesh and Sultan 2 is the weight percent of Bi is much greater for Sultan 2 (56-58%) than Red Flesh (40%). In general, the distributions of the Bi phase in both homogeneous assemblies are similar. There are two distinct Bi precipitate morphologies, with large primary Bi particles and small plate-like precipitates. Sultan 2 has more prominent large primary Bi precipitates and finer, close spaced plate-like precipitates. These findings are consistent with the work of Belyakov et al. who identified two types of Bi phases in Bi containing solders. They described the two Bi morphologies as large, chunky Bi particles that form in the grain boundary during solidification and as small Bi plates that precipitate in the solid state [53].

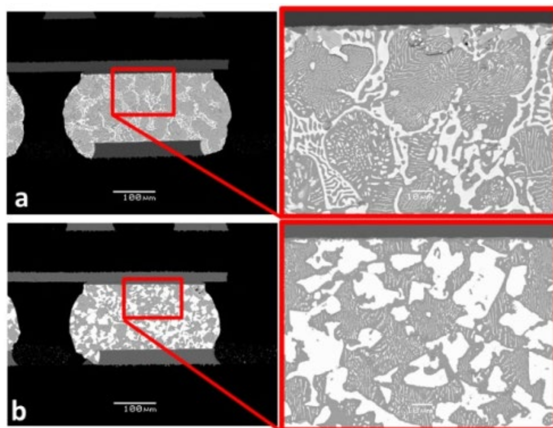

Figure 6. Cross sectional solder joint images of as-assembled CTBGA84 a) homogeneous Red Flesh and b) homogeneous Sultan 2 before thermal cycling (results published previously [61]).

Accelerated Temperature Cycling Results

This section includes the CTBGA84 component Accelerated Temperature Cycling (ATC) Weibull statistics, distribution plots and a summary analysis of the data, comparing results of the 0/100 °C with the -15/85 °C thermal cycling profiles.

Figure 7 is a bar chart comparing the characteristic lifetime statistics, and Figure 8 is a bar chart comparing the 1% cumulative failure statistics, for all LTS alloy test legs from the 0/100 °C (results published previously [61]) and -15/85 °C ATC profiles. Figure 9 and Figure 10 are bar charts including the 1% cumulative failure and characteristic lifetime statistics from the 0/100 °C (results published previously [61]) and -15/85 °C thermal cycling profiles respectively.

Figure 11 are composite Weibull distribution plots for all test legs from the -15/85 °C ATC profile (the bottom plot includes 90% confidence intervals). Figure 12 are two Weibull distribution plots, for the hybrid Red Flesh, hybrid Sultan 2 and SAC305 baseline legs from the -15/85 °C ATC profile (the bottom plot includes 90% confidence intervals). Figure 13 are two Weibull distribution plots, for the homogeneous Red Flesh, homogeneous Sultan 2 and SAC305 baseline legs from the -15/85 °C ATC profile (the bottom plot includes 90% confidence intervals). Figure 14 are two Weibull distribution plots, for the hybrid Beserah JRP, hybrid Golden Pillow 2 JRP and SAC305 baseline legs from the -15/85 °C ATC profile (the bottom plot includes 90% confidence intervals). The Weibull statistics for both ATC profiles are then summarized in Table 1 (results for 0/100 °C were published previously [61]).

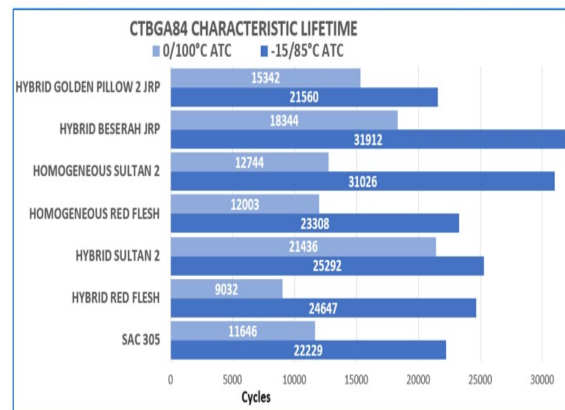

Figure 7. A bar chart comparing the characteristic lifetime statistics of the CTBGA84 component for all LTS alloy test legs from the 0/100 °C (results published previously [61]) and -15/85 °C ATC profiles.

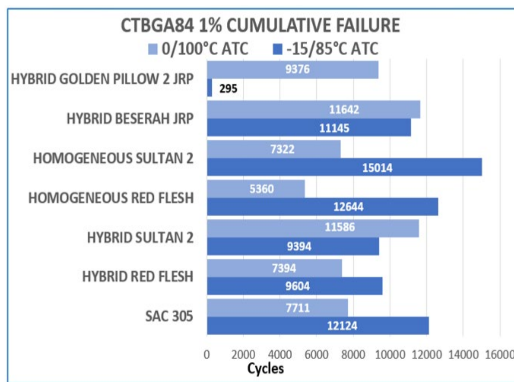

Figure 8. A bar chart comparing the 1% cumulative failure statistics of the CTBGA84 component for all LTS alloy test legs from the 0/100 °C (results published previously [61]) and -15/85 °C ATC profiles.

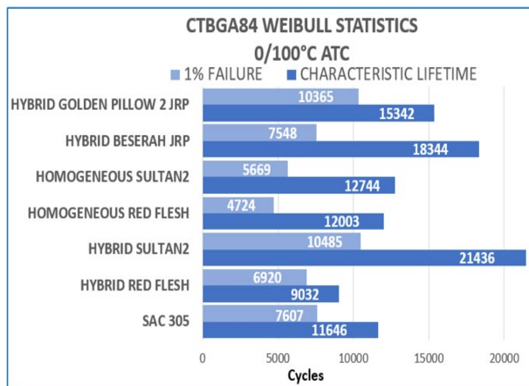

Figure 9. A bar chart showing the CTBGA84 component 1% cumulative failure and characteristic lifetime statistics from the 0/100 °C ATC profile (results published previously [61]).

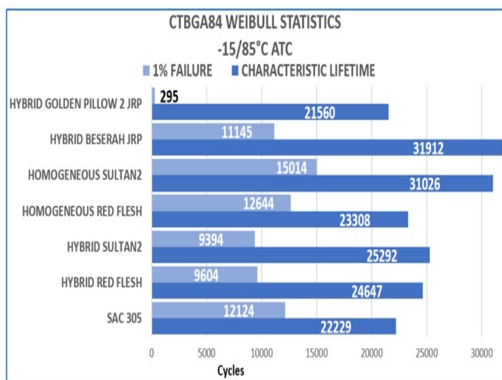

Figure 10. A bar chart showing the CTBGA84 component 1% cumulative failure and characteristic lifetime statistics from the -15/85 °C ATC profile.

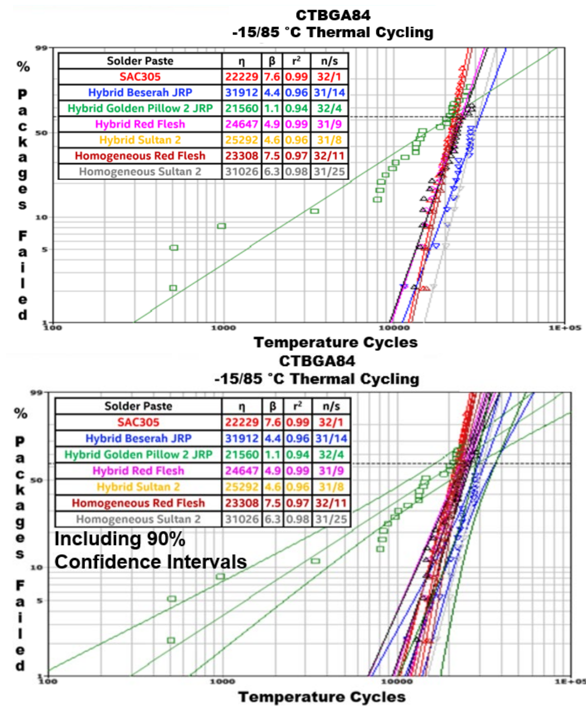

Figure 11. CTBGA84 composite Weibull distribution plots showing thermal cycling results for all 6 LTS legs and the SAC305 baseline from the -15/85 °C ATC profile (the bottom plot includes 90% confidence intervals).

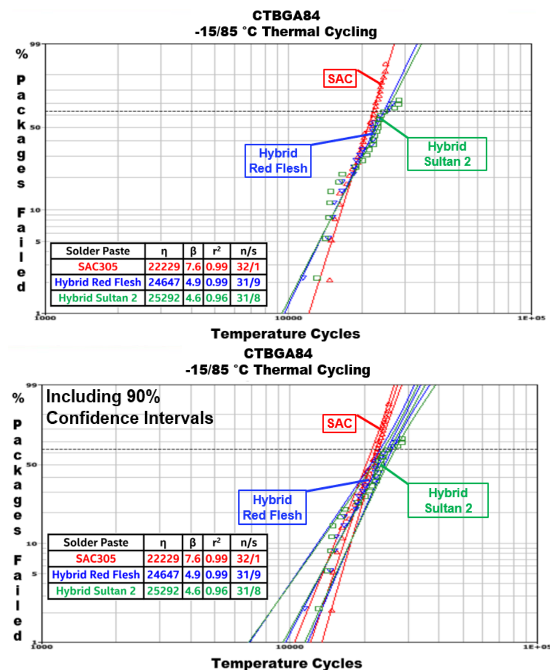

Figure 12. CTBGA84 Weibull distribution plots showing thermal cycling results for hybrid Red Flesh, hybrid Sultan 2 and SAC305 baseline from the -15/85 °C ATC profile (the bottom plot includes 90% confidence intervals).

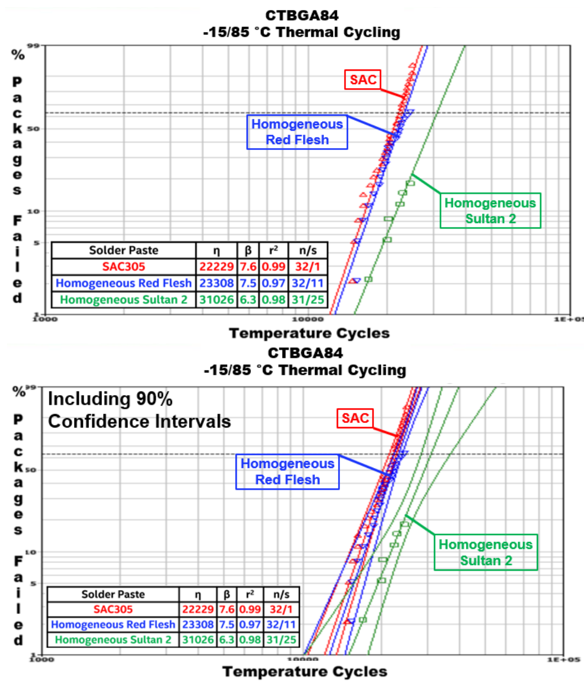

Figure 13. CTBGA84 Weibull distribution plots showing thermal cycling results for homogeneous Red Flesh, homogeneous Sultan 2 and SAC305 baseline from the -15/85 °C ATC profile (the bottom plot includes 90% confidence intervals).

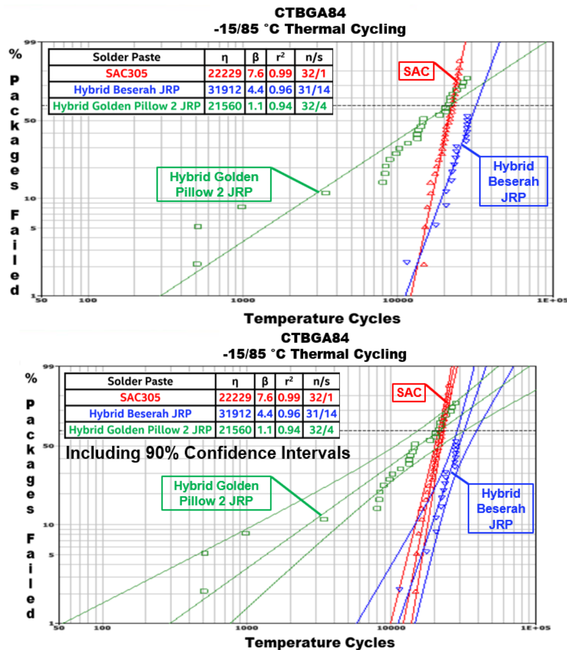

Figure 14. CTBGA84 Weibull distribution plots showing thermal cycling results for hybrid Beserah JRP, hybrid Golden Pillow 2 JRP and SAC305 baseline from the -15/85 °C ATC profile (the bottom plot includes 90% confidence intervals).

Table 1. Summary of Weibull statistics for the CTBGA84 component run in the 0/100 °C ATC profile (results published previously [61]) and in the -15/85C °C ATC profile.

CTBGA84 Weibull Statistics for 0/100 °C Thermal Cycling				
Solder Assembly Type	Characteristic Lifetime η (cycles)	1% Failures (cycles)	Slope β	Correlation Coefficient, r^2
SAC Baseline	**11646**	**7607**	**10.8**	**0.90**
Hybrid Red Flesh	9032	6920	17.3	0.77
Hybrid Sultan 2	21436	10485	8.0	0.89
Homogeneous Red Flesh	12003	4724	4.9	0.83
Homogeneous Sultan 2	12744	5669	5.7	0.82
Hybrid Beserah Joint Reinforced Paste	18344	7548	5.2	0.95
Hybrid Golden Pillow 2 Joint Reinforced Paste	15342	10365	11.7	0.97

CTBGA84 Weibull Statistics for -15/85 °C Thermal Cycling				
Solder Assembly Type	Characteristic Lifetime η (cycles)	1% Failures (cycles)	Slope β	Correlation Coefficient, r^2
SAC Baseline	**22229**	**12124**	**7.6**	**0.99**
Hybrid Red Flesh	24647	9604	4.9	0.99
Hybrid Sultan 2	25292	9394	4.6	0.96
Homogeneous Red Flesh	23308	12644	7.5	0.97
Homogeneous Sultan 2	31026	15014	6.3	0.98
Hybrid Beserah Joint Reinforced Paste	31912	11145	4.4	0.96
Hybrid Golden Pillow 2 Joint Reinforced Paste	21560	295	1.1	0.94

From the Weibull characteristic lifetime analysis shown in Table 1 and Figures 7-14, all LTS legs in the less aggressive -15/85 °C profile had comparable or exceeded the characteristic lifetime performance of the SAC305 baseline, when adding 90% confidence intervals. In the more aggressive 0/100 °C profile, all LTS legs had comparable or exceeded the characteristic lifetime performance of the SAC305 baseline, when adding 90% confidence intervals, except for hybrid Red Flesh which had a lower characteristic lifetime performance (as presented in a previous publication [61]).

From the Weibull 1% cumulative failure analysis shown in Table 1 and Figures 7-14, when adding 90% confidence intervals in the less aggressive -15/85 °C profiles, all LTS legs had comparable 1% cumulative failure performance except for hybrid Golden Pillow 2 JRP, which had a very different slope than the other legs (β=1.1), with first failures starting as early as 507 cycles. In the more aggressive 0/100 °C profile, all LTS legs had comparable or exceeded the 1% cumulative failure performance of the SAC305 baseline, when adding 90% confidence intervals, except for homogeneous Red Flesh which had a lower 1% cumulative failure performance (as presented in a previous publication [61]).

The early 1% cumulative failures, in the -15/85 °C profile hybrid Golden Pillow 2 leg, indicate a time zero SMT quality defect (HoP-like solder joints as shown in Figure 2). These defects are believed to form by the premature gelling of the resin in the JRP paste before the solder has become molten

and has wet the BGA SAC sphere. Increasing the initial reflow profile ramp rate to >3°C/sec (from 1-2°C/sec) for the Golden Pillow 2 leg is one suggested method to eliminate these defects [22].

Table 2. CTBGA84 component characteristic lifetime ratio comparison of the 0/100 °C ATC profile (results published previously [61]) and the -15/85 °C ATC profile.

CTBGA84 WEIBULL STATISTICS ; CHARACTERISTIC LIFETIME			
THERMAL CYCLE PROFILE RATIO COMPARISON			
LEG NAME	0/100°C ATC PROFILE	-15/85°C ATC PROFILE	RATIO = $\frac{-15/85\ °C}{0/100\ °C}$
SAC Baseline	**11646**	**22229**	**1.9X**
Hybrid Red Flesh	9032	24647	2.7X
Hybrid Sultan 2	21436	25292	1.2X
Homogeneous Red Flesh	12003	23308	1.9X
Homogeneous Sultan 2	12744	31026	2.4X
Hybrid Beserah JRP	18344	31912	1.7X
Hybrid Golden Pillow 2 JRP	15342	21560	1.4X
		Average	**1.9X**

Table 2 shows the CTBGA84 component characteristic lifetime ratio comparisons, which were calculated by dividing the characteristic lifetime of the -15/85 °C thermal cycling profile leg by the characteristic lifetime of the 0/100 °C profile leg. The results show the factor by which the -15/85 °C characteristic lifetime was either increased or decreased relative to the 0/100 °C characteristic lifetime for each leg. For example, if an alloy had the same characteristic lifetime performance across the two different ATC profiles, the ratio would result in 1X. This analysis shows that all CTBGA84 component LTS legs had characteristic lifetime increases of 1.9X on average in the -15/85 °C profile than in the 0/100 °C profile, which is the same amount that the SAC305 Baseline characteristic lifetime was extended (1.9X). Hybrid Red Flesh (2.7X), homogeneous Sultan 2 (2.4X) and homogeneous Red Flesh (1.9X) were all increased beyond the SAC305 baseline characteristic lifetime ratio, while hybrid Sultan 2 (1.2X), hybrid Golden Pillow 2 JRP (1.4X), and hybrid Beserah JRP (1.7X) were all decreased.

Table 3. CTBGA84 component 1% cumulative failure ratio comparison of the 0/100 °C ATC profile (results published previously [61]) and the -15/85 °C ATC profile.

CTBGA84 WEIBULL STATISTICS ; 1% CUMULATIVE FAILURE			
THERMAL CYCLE PROFILE RATIO COMPARISON			
LEG NAME	0/100°C ATC PROFILE	-15/85°C ATC PROFILE	RATIO = $\frac{-15/85\ °C}{0/100\ °C}$
SAC Baseline	**7711**	**12124**	**1.57X**
Hybrid Red Flesh	7394	9604	1.30X
Hybrid Sultan 2	11586	9393	0.81X
Homogeneous Red Flesh	5360	12644	2.36X
Homogeneous Sultan 2	7322	15014	2.05X
Hybrid Beserah JRP	11642	11145	0.96X
Hybrid Golden Pillow 2 JRP	9376	295	0.03X

Table 3 shows the CTBGA84 component 1% cumulative failure ratio comparisons, which were calculated by dividing the 1% cumulative failure of the -15/85 °C thermal cycling profile leg by the 1% cumulative failure of the 0/100 °C profile leg. The results show the factor by which the -15/85 °C 1% cumulative failure was either increased or decreased relative to the 0/100 °C 1% cumulative failure for each leg. For example, if an alloy had the same 1% cumulative failure performance across the two different ATC profiles, the ratio would result in 1X. This analysis shows that the CTBGA84 component SAC305 baseline 1% cumulative failure was increased by 1.57X in the -15/85 °C profile then the 0/100 °C profile. Homogenous Red Flesh (2.36X) and homogeneous Sultan 2 (2.05X) were both increased beyond the SAC305 baseline 1% cumulative failure ratio, while hybrid Red Flesh (1.30X), hybrid Beserah JRP (0.96X), hybrid Sultan 2 (0.81X) and hybrid Golden Pillow 2 JRP (0.03X) were all decreased.

Failure Mode Analysis

The microstructural response of SAC solder joints during thermal cycling is well known. The coarsening of the network of Ag_3Sn precipitates is followed by recrystallization and propagation of cracks along the newly formed Sn grain boundaries. BGA thermal fatigue failures in Sn-based solders typically have a crack path through the strain-localized region of the bulk solder, although propagation may proceed close to the IMC interfacial layer. The fracture path is characterized by local recrystallization, global recrystallization, crack branching, and cavitation at boundary triple points (for example, at the triple junction between the solder, land and solder mask). These are common fracture characteristics for SAC solder thermal fatigue failures and are consistent with those reported first by Dunford in 2004 [54] and confirmed in many previous publications [37, 41, 42, 43, 55, 56, 61, 62].

Figure 15 shows backscattered SEM image of two thermal cycled solder joints from a CTBGA84 SAC305 baseline sample, -15/85 °C profile. Crack initiation and propagation is within the bulk solder close to the package side interface. Mostly partial cracking was observed near the PCB interface. This aligns with similar results from the 0/100 °C profile (results published previously [61]).

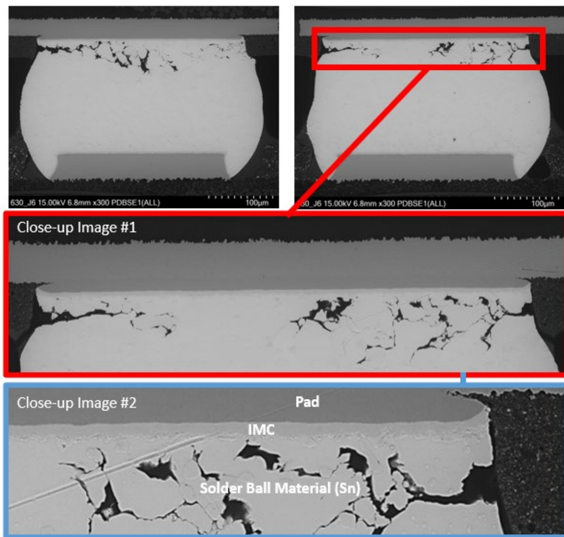

Figure 15. Backscattered SEM images of two thermal cycled solder joints from a CTBGA84 SAC305 baseline sample, -15/85 °C ATC profile (electrical failure detected at 15,019 cycles, removed from the chamber at 19,000 cycles).

Figures 16 through 21 show thermally cycled solder joints from the hybrid, homogeneous, and hybrid JRP CTBGA84 samples from the -15/85 °C profile. In general, most hybrid test legs exhibit the same basic failure characteristics of the SAC305 baseline, with thermal fatigue cracking through the bulk solder near the package side. However, there is some evidence of mixed mode failures, which is a combination of solder fatigue and interfacial cracking. Mixed mode failures are shown in hybrid Red Flesh, -15/85 °C (Figure 16), hybrid Sultan 2, 0/100 °C (results published previously [61]), Beserah JRP, -15/85 °C (Figure 20) and Beserah JRP, 0/100 °C (results published previously [61]).

It is noteworthy that hybrid Red Flesh (Figure 16, 40% weight percent of Bi) shows Bi particles in the package side region, in the -15/85 °C profile. The predominant fatigue failure location is at the package side in the unmelted SAC region. Less fatigue cracking was detected in the Bi-mixed region of some hybrid and JRP solder joints. Mostly partial cracking was observed in the Bi rich region near the PCB interface in some JRP and hybrid solder joints. This is consistent with Weibull plots for the hybrid and JRP assemblies that show no evidence of a bimodal distribution indicative of more than a single solder joint failure mechanism or crack propagation path. An example of a thermal fatigue failure in a Bi mixed region is shown in the lower image of Figure 20 (hybrid Beserah JRP) -15/85 °C ATC profile. The crack likely initiates at an incoherent boundary between Bi and Sn phases and propagates either along Sn grain boundaries, along a phase boundary between Bi precipitates and the Sn matrix, or through a large, coarsened Bi phase that has accumulated near the intermetallic (IMC) layer.

Figures 18-19 show failures in homogeneous Red Flesh and homogeneous Sultan 2 solder joints. Homogeneous solder joints fail in the strain localized region near the package side. The cracks likely initiate at an incoherent boundary between Bi and Sn phases and propagate either along Sn grain boundaries, along a phase boundary between Bi precipitates and the Sn matrix, or through a large, coarsened Bi phase that has accumulated near the intermetallic (IMC) layer. This aligns with similar results from the 0/100 °C profile (results published previously [61]).

Figures 18-19 also show voids in the failed CTBGA84 homogeneous solder alloy assemblies. The voiding is located at adjoining large Bi precipitates or at Bi/Sn interfaces. Because minimal voiding was detected before thermal cycling (Figure 4), it is assumed that the voids formed during thermal cycling [57]. During thermal cycling, saturated Bi that is in solid solution in the Sn matrix transforms into a secondary Bi precipitate. It has been estimated that the precipitation of Bi causes about a 25% reduction in the localized volume [57]. This volume misfit generates an elastic strain energy that is proportional to the volume change during the phase transformation of precipitation. In turn, a tensile stress is introduced at the boundary between the Bi precipitate and the Sn matrix. This eventually causes separation between the phases resulting in the formation of a void [58]. This process is analogous to the cavitation voiding at boundary triple points in SAC solders that is responsible for tertiary creep during thermal cycling [54, 59].

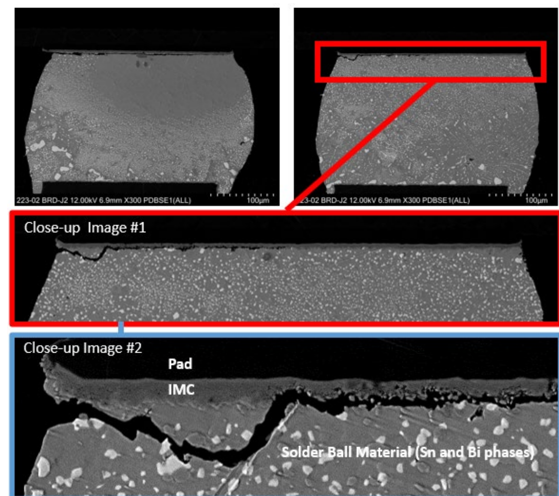

Figure 16. Backscattered SEM images of two thermal cycled solder joints from a CTBGA84 hybrid Red Flesh sample, -15/85 °C ATC profile (electrical failure detected at 20,158 cycles, removed from the chamber at 27,908 cycles).

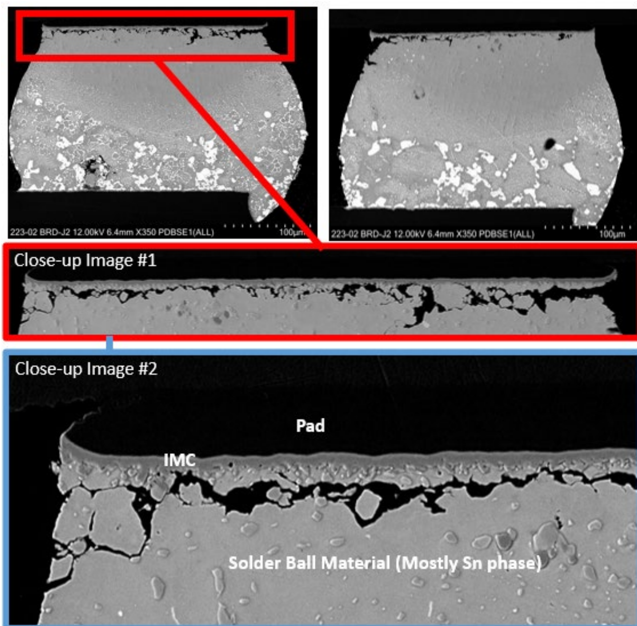

Figure 17. Backscattered SEM images of two thermal cycled solder joints from a CTBGA84 hybrid Sultan 2 sample, -15/85 °C ATC profile (electrical failure detected at 22,617 cycles, removed from the chamber at 27,908 cycles).

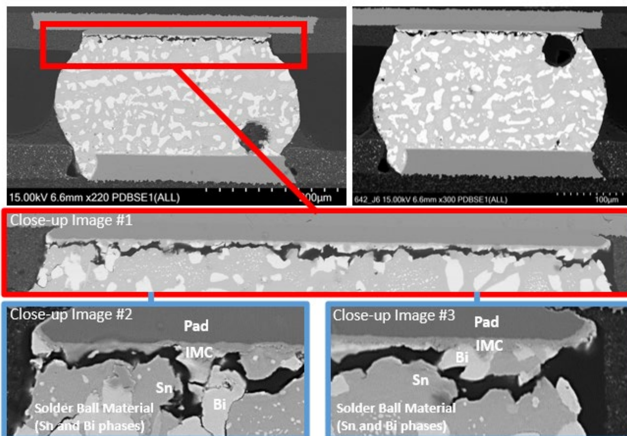

Figure 18. Backscattered SEM images of two thermal cycled solder joints from a CTBGA84 homogeneous Red Flesh sample, -15/85 °C ATC profile (electrical failure detected at 15,411 cycles, removed from the chamber at 15,500 cycles).

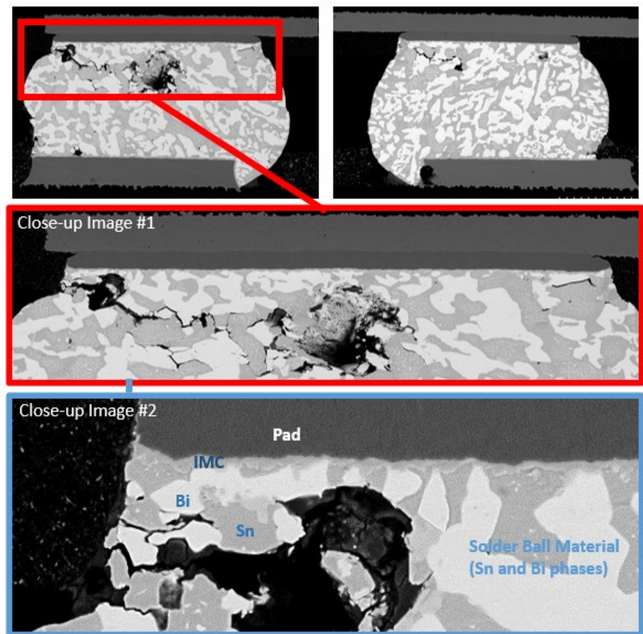

Figure 19. Backscattered SEM images of two thermal cycled solder joints from a CTBGA84 homogeneous Sultan 2 sample, -15/85 °C ATC profile (electrical failure detected at 22,513 cycles, removed from the chamber at 24,408 cycles).

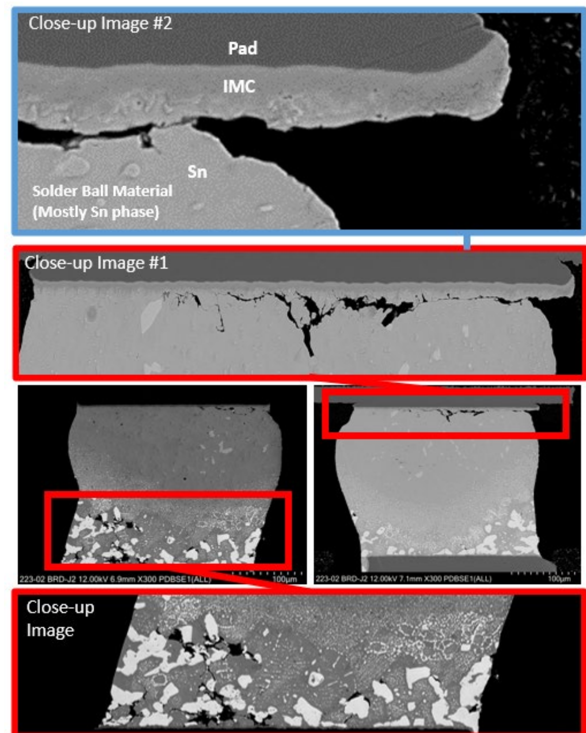

Figure 20. Backscattered SEM images of two thermal cycled solder joints from a CTBGA84 hybrid Beserah JRP sample, -15/85 °C ATC profile (electrical failure detected at 23,883 cycles, removed from the chamber at 27,908 cycles).

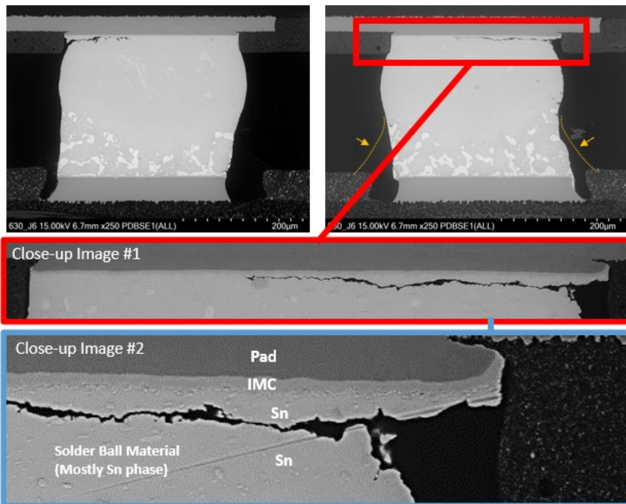

Figure 21. Backscattered SEM images of two thermal cycled solder joints from a CTBGA84 hybrid Golden Pillow 2 JRP sample, -15/85 °C ATC profile (electrical failure detected at 13,345 cycles, removed from the chamber at 19,000 cycles).

SUMMARY

The thermal fatigue resistance of six Low Temperature Solder (LTS) alloys was assessed using a CTBGA84 ball grid array test vehicle and accelerated thermal cycling profiles of 0 to 100 °C (IPC-9701B, TC1) and -15 to 85 °C. The original concern with the accelerated 0/100 °C thermal profile was that the Bi-Sn might not perform as well with the higher acceleration provided at an upper temperature extreme of 100 °C. As 100 °C is close to the onset of the low temperature solder melting temperature, it may result in a decrease in the strength of the solder, possibly lowering the characteristic lifetime. Additionally, most computer products, used by consumers, do not operate continuously at 100 °C. For both reasons, another profile with a lower upper temperature extreme was also used for this study. Thus the -15/85 °C accelerated profile was selected due to homologous temperature considerations between Sn-Ag-Cu and Bi-Sn solder and maintaining a similar delta T [100° C] across both ATC profiles.

From the Weibull characteristic lifetime analysis of the CTBGA84 component, all LTS legs in the -15/85 °C profile had comparable or exceeded the characteristic lifetime performance of the SAC305 baseline, when adding 90% confidence intervals. In the more aggressive 0/100 °C profile, all LTS legs had comparable or exceeded the characteristic lifetime performance of the SAC305 baseline, when adding 90% confidence intervals, except for hybrid Red Flesh which had a lower characteristic lifetime performance (as presented in a previous publication [61]).

From the Weibull 1% cumulative failure analysis of the CTBGA84 component, when adding 90% confidence intervals in the -15/85 °C profiles, all LTS legs had comparable 1% cumulative failure performance except for hybrid Golden Pillow 2 JRP, which had a very different slope than the other legs (β=1.1), with first failures starting as early as 507 cycles. These early 1% cumulative failures indicate a time zero SMT quality defect (HoP-like solder joints). These defects are believed to form by the premature gelling of the resin in the JRP paste before the solder has become molten and has wet the BGA SAC sphere. Increasing the initial reflow profile ramp rate to >3°C/sec (from 1-2°C/sec) for the Golden Pillow 2 leg is one suggested method to eliminate these defects [22].

In the more aggressive 0/100 °C profile, all CTBGA84 component LTS legs had comparable or exceeded the 1% cumulative failure performance of the SAC305 baseline, when adding 90% confidence intervals, except for homogeneous Red Flesh which had a lower 1% cumulative failure performance (presented in previous publication [61]).

Metallographic cross-sectional failure analysis on the CTBGA84 component, from both ATC profiles, showed that fatigue cracking near the package side within the bulk solder was the predominant failure mode. However, some mixed mode interfacial/fatigue failures were detected in some of the hybrid test legs. Non-fatigue failures in hybrid solder joints may be related to Bi diffusion into the SAC region during thermal cycling, which strengthens the SAC solder. Fatigue cracking at the package side in the SAC region is found to initiate at boundary triple points and propagate in solder material, which is commonly characterized by local recrystallization, global recrystallization, crack branching, and cavitation at boundary triple points [37, 41, 42, 43, 54, 55, 56, 61, 62].

A much smaller amount of fatigue cracking was detected in the Bi-mixed region of hybrid and JRP solder joints. The fatigue cracking at the PCB side in the Bi-mixed region proceeds typically along phase boundaries, recrystallized Sn grains, and occasionally by cleavage through Bi precipitates.

FUTURE WORK

At the time of writing this interim paper, two of the -15/85 °C profile legs had not yet reached the N63 failure criteria per IPC-9701B. This experiment will continue running until the failure criteria is reached. The Weibull information will then be updated at that time.

ACKNOWLEDGEMENTS
The iNEMI LTSPD project achievements rely heavily on the engagement, great effort and contribution of the whole participating project team members. These members include engineers from the following corporations: Intel, Celestica, Wistron, IBM, Lenovo, Nokia, HP, Flex, Indium, Senju, MacDermid Alpha Electronics Solutions, Interflux, Eunow, Shinko Electric Industries, Nihon Superior, Heraeus, Dell, Keysight, Abbott, Safran, Binghamton University, and Purdue University. The LTSPD Project Team also acknowledges the in-kind contribution of materials, components, and PCBs to our project from ASE, FIT, ITEQ, Lotes, Molex, Panasonic, Tamura, Tripod, Yincae, Shengyi Technology and Shengyi Electronics. iNEMI also acknowledges the contributions for accelerated temperature cycling, test monitoring, and analytical support from the management of Nokia Bell Labs in Murray Hill, NJ and the management of Intel's CQN Lab in Folsom, CA and Intel's Failure Analysis Lab in Hillsboro, OR.

REFERENCES
[1] Shubhada Sahasrabudhe, Scott Mokler, Mukul Renavikar, Sandeep Sane, Kevin Byrd, Eric Brigham, Owen Jin, Pubudu Goonetilleke, Nilesh Badwe and Satish Parupalli, "Low Temperature Solder – A Breakthrough Technology for Surface Mounted Devices," *Proceedings 68th Electronic Components and Technology Conference*, 1455-1464, San Diego, CA, May 29-June 1, 2018.
[2] R. Aspandiar, K. Byrd, K.K. Tang, L. Campbell, and S. Mokler, "Investigations of Low Temperature Solders to Reduce Reflow Temperature, Improve SMT Yields and Realize Energy Savings," *Proceedings of the 2015 APEX Conference*, San Diego, CA, February 2015.
[3] Scott Mokler, Raiyo Aspandiar, Kevin Byrd, Olivia Chen, Satyajit Walwadkar, Kok Kwan Tang, Mukul Renavikar and Sandeep Sane, "The Application of Bi-Based Solders for Low Temperature Reflow to Reduce Cost while Improving SMT Yields in Client Computing System, *Proceedings of SMTAI 2016*, 318-326, Rosemont, IL, September 2016.
[4] Max Hansen, **Constitution of Binary Alloys**, 2nd edition, McGraw-Hill, 1175-1177, 1958.
[5] H. Kang, S. H. Rajendran, J. P. Jung, "Low Melting Temperature "Sn-Bi Solder: Effect of Alloying and Nanoparticle Addition on the Microstructural, Thermal, Interfacial Bonding, and Mechanical Characteristics." *Metals* 11, 364, 2021.
[6] Raiyo Aspandiar, Nilesh Badwe, and Kevin Byrd, "Chapter 5: Low Temperature Lead-Free Alloys and Solder Pastes," **in Lead-free Soldering Process Development and Reliability**, Jasbir Bath, editor, 95-154, John Wiley & Sons, Inc. Print July 28, 2020, ISBN 9781119482031, online July 3, 2020, ISBN 9781119482093.
[7] Y. Liu and K.N. Tu, "Low melting point solders based on Sn, Bi, and In elements," *Materials Today Advances*, 1-16, 8, 100115, 2020.
[8] Fengjiang Wang, Hong Chen, Yiang Huang, Luting Liu, and Zhijie Zhang, "Recent progress on the development of Sn-based low-temperature Pb-free solders," *J. Materials Science: Materials in Electronics*, 30, 3222-3243, 2019.
[9] Morgana Ribas, Tom Hunsinger, Traian Cucu, Ramakrishna H V, Garian Lim and Mike Murphy, **The Printed Circuit Assembler's Guide to Low-Temperature Soldering**, I-Connect007, eBook ISBN: 978-0-9998648-4-5, © 2018 BR Publishing, Inc., Rohnert Park, CA 94927, U.S.A.
[10] Hiren R. Kotadia, Philip D. Howes, Samjid H. Mannan, "A review: On the development of low melting temperature Pb-free solders," *Microelectronics Reliability*, 54, 1253-1273, 2014.
[11] F. Hua, Z. Mei and J. Glazer, "Eutectic Sn-Bi as an Alternative as to Pb-Free Solders", Proceedings of the IEEE Electronic Components and Technology Conference (ECTC), 277-283. 1998
[12] NCMS Report 0401RE96, "Lead-Free Solder Project – Final Report", National Center for Manufacturing Sciences (NCMS), August 1997.
[13] K-W. Moon, W.J. Boettinger, U.R. Kattner, C.A. Handwerker, D-J Lee, "The Effect of Pb Contamination on the Solidification Behavior of Sn-Bi Solders", J. Electron. Mater., 30(1), 45-52. 2001,
[14] J. Glazer, "Microstructure and Mechanical Properties of Pb-Free Solder Alloys for Low-Cost Electronic Assembly" A Review". J. Electron. Mater., 23(8), 1994, pp. 693-700.
[15] E. Ferrer, H. Holder, "57Bi-42Sn-1Ag: A Lead Free, Low Temperature Solder for the Electronic Industry," IPC JEDEC 4th International Conference on Lead-Free Electronic Components and Assemblies, San Jose, CA, March 22-25, 2003.
[16] J. Wang, L. Wen, J. Zhou, and M. Chung, "Mechanical Properties and Joint Reliability Improvement of Sn-Bi Alloy," *Proceedings of the IEEE Electronic Components and Technology Conference (ECTC)*, 492-496, 2011.
[17] O. H. Chen, K. Byrd, S. Mokler, K. K. Tang, and R. Aspandiar, "Comparison Of The Mechanical Shock/Drop Reliability Of Flip Chip BGA (FCBGA) Solder Joints Formed By Soldering With Low Temperature BiSn-Based Resin Reinforced Solder Pastes," *Proceedings of the 2015 International Conference on Soldering and Reliability (ICSR)*, Toronto, Canada, May 2015.
[18] O. H. Chen, A. Molina, R. Aspandiar, K. Byrd, S. Mokler, and K. K. Tang, "Mechanical Shock and Drop Reliability Evaluation of the BGA Solder Joint Stack-Ups Formed by Reflow Soldering SAC Solder Balls BGAs With BiSnAg And Resin Reinforced BiSn-Based Solder Pastes," *Proceedings of the 2015 SMTA International Conference*, 215-222, Rosemont, IL, September 2015.

[19] O. H. Chen, J. Gao, T. C.C. Pan, K. K. Tang, R. Aspandiar, K. Byrd, B. Zhou, S. Mokler, and A. Molina, "Solder Joint Reliability on Mixed SAC-BiSn Ball Grid Array Solder Joints Formed with Resin Reinforced Bi-Sn Metallurgy Solder Pastes," *Proceedings of the 2016 SMTA International Conference*, 216-228, Rosemont, IL, September 2016.

[20] R. Coyle, R. Aspandiar, M. Osterman, C. Johnson, R. Popowich, R. Parker and D. Hillman, "Thermal Cycle Reliability of a Low Ag Ball Grid Array Assembled with Tin Bismuth Solder Paste," *Proceedings of 2017 SMTA International Conference*, 72-83, Rosemont, IL, September 2017.

[21]https://news.lenovo.com/pressroom/press-releases/lenovo-announces-breakthrough-innovative-pc-manufacturing-process/ Lenovo™ Announces Breakthrough, Innovative PC Manufacturing Process.

[22] Haley Fu, Jagadeesh Radhakrishnan, Pubudu Goonetilleke, Kei Murayama, Raiyo Aspandiar, Babak Arfaei, Kevin Byrd, Antonio Caputo, Jimmy Chen, Qin Chen, Richard Coyle, Derek Daily, Sophia Feng, Carol Handwerker, Ralph Lauwaert, Francis Mutuku, Morgana Ribas, Murali Sarangapani, Kok Kwan Tang, Kris Troxel, Vasu Vasudevan, Daniel Werkhoven, Greg Wu, Hongwen Zhang, Wilson Zhen, "iNEMI Project on Process Development of BiSn-based low temperature solder pastes - Part VII: Mechanical Shock Test and Failure Analysis on Mixed SnAgCu-BiSn Solder Joints of FCBGA Components," *Proceedings of the 2020 SMTA International Virtual Conference*, September 2020.

[23] M. Ribas, P. Augustine, P. Choudhury, R.R. Rangaraju, A. Kumar, S. Sarkar, "Low Temperature Soldering: Thermal Cycling Reliability Performance," *Proceedings of the 2019 APEX Conference,* S05-02, San Diego, CA, February 4-6, 2019.

[24] H. Fu, J. Radhakrishnan, M. Ribas, R. Aspandiar, B. Arfaei, K. Byrd, A. Caputo, J. Chen, S. Cheng, Q. Chen, R. Coyle, D. Daily, S. Feng, P. Goonetilleke, R. Lauwaert, F. Mutuku, M. Sarangapani, K. K. Tang, K. Troxel, D. Werkhoven, G. Wu, A. Zhang, W. Zhen, "iNEMI Project on Process Development of BiSn-based low temperature solder pastes - Part VI: Mechanical Shock Results of Resin Reinforced Mixed SnAgCu-BiSn Solder Joints of FCBGA Components", *Proceedings of the 2019 SMTA International Conference*, Rosemont, IL, October 2019.

[25] Pritha Choudhury, Morgana Ribas, Raghu Raj Rangaraju and Siuli Sarkar, "High Reliability Low Temperature Solder Alloys, " *Proceedings of the 2019 SMTA International Conference,* Rosemont, IL, October 2019.

[26] H. Fu, J. Radhakrishnan, M. Ribas, R. Aspandiar, K. Byrd, J. Chen, S. Cheng, Q. Chen, R. Coyle, S. Feng, B. Hardin, M. Krmpotich, S. Mokler, B. Sandy-Smith, K. K. Tang, G. Wu, A. Zhang, and W. Zhen, "iNEMI Project on Process Development of BiSn-Based Low Temperature Solder Pastes – Part III: Mechanical Shock Tests on POP BGA Assemblies", *Proceedings of the 2018 International Conference on Electronics Packaging (IECP)*, Kuwana, Japan, April, 2018.

[27] M. Ribas, S. Chegudi, A. Kumar, R. Pandher, R. Raut, S. Mukherjee, S. Sarkar, and B. Singh, "Development of Low-Temperature Drop Shock Resistant Solder Alloys for Handheld Devices," *Proceedings of the IEEE 15th Electronics Packaging Technology Conference*, 53-57, Singapore. December 2013.

[28] Chongyang Cai, Jiefeng Xu, Huayan Wang, S.B. Park, "A comparative study of thermal fatigue life of Eutectic Sn-Bi, Hybrid Sn-Bi/ SAC and SAC solder alloy BGAs," *Microelectronics Reliability*, vol. 119, 2021. https://doi.org/10.1016/j.microrel.2021.114065.

[29] Charmaine Johnson, Richard Coyle, Martin Anselm, Lenora Clark, Ajitesh Singh Parihar, Richard Popowich, Tayler Swanson, Jason Fullerton, and Chen Xu, "Attachment Quality and Thermal Fatigue Reliability of a Surface Mount Chip Resistor Assembled with a Low Temperature Solder," *Proceedings of SMTAI*, 457-464, Rosemont, IL, September 2019.

[30] Richard Coyle, Martin Anselm, Faramarz Hadian, Sahana Kempaiah, Anto Raj, Richard Popowich, Lenora Clark, Jason Fullerton, and Charmaine Johnson, "The Effect of Peak Reflow Temperature on Thermal Cycling Performance and Failure Mode of Hybrid Low Temperature Solder Joints," *Proceedings of SMTAI 2021*, 386-399, Minneapolis, MN, November 2021.

[31] Luke Wentlent, James Wilcox, and Michael Meilunas, "Thermal Cycling Behaviors of Hybrid and Homogeneous Low Temperature Solder Interconnects," *Proceedings of SMTAI 2021*, 547-563, Minneapolis, MN, November 2021.

[32] Sahana Marur Kempaiah, Martin K Anselm, Richard Coyle, and Faramarz Hadian, "Thermal Reliability of Mixing Bismuth-Containing Solder Paste with SAC BGAs at Low Reflow Temperatures - Part II," *Proceedings of SMTAI 2021*, 478-485, Minneapolis, MN, November 2021.

[33] Andrew Mawer, Mollie Benson, A.R. Nazmus Sakib, Nihaar Mahatme, Anirban Roy, Paul Ngan, and Catherine Pronga, "Hybrid Assembly and Reliability of Conventional Pb-Free BGAs Using Low Temperature Solder Paste for Temperature Sensitive IC Applications," *Proceedings of SMTAI 2021*, 486-494, Minneapolis, MN, November 2021.

[34] Kevin Byrd, Jason Stafford, Prithvi Kotian, Pubudu Goonetilleke, and Brian Franco, "SAC-SnBi Solder Joint Failure Location vs. Acceleration Condition," *Proceedings of SMTAI 2021*, 366-371, Minneapolis, MN, November 2021.

[35] Haley Fu, Raiyo Aspandiar, Jimmy Chen, Shunfeng Cheng, Qin Chen, Richard Coyle, Sophia Feng, Bill Hardin, Mark Krmpotich, Scott Mokler, Jagadeesh Radhakrishnan, Morgana Ribas, Brook Sandy-Smith, Kok Kwan Tang, Greg

Wu, Anny Zhang, Wilson Zhen, "iNEMI Project on Process Development of BiSn-Based Low Temperature Solder Pastes *Proceedings of SMTA International*, 207-220, September 7 - 21, 2017, Rosemont, IL.
[36] Haley Fu, Raiyo Aspandiar, Jimmy Chen, Shunfeng Cheng, Qin Chen, Richard Coyle, Sophia Feng, Bill Hardin, Mark Krmpotich, Scott Mokler, Jagadeesh Radhakrishnan, Morgana Ribas, Brook Sandy-Smith, Kok Kwan Tang, Greg Wu, Anny Zhang, Wilson Zhen, "iNEMI Project on Process Development of BiSn-Based Low Temperature Solder Pastes: Characterization of Mixed Alloy BGA Solder Joints, *Proceedings of Pan Pacific Microelectronics Symposium*," February 5-8, 2018, Hawaii, HI.
[37] Richard Coyle, Raiyo Aspandiar, Faramarz Hadian, Sahana Kempaiah, Vasu Vasudevan, Aileen Allen, Anto Raj, Pubudu Goonetilleke, Dan Burkholder, Morgana Ribas, Jagadeesh Radhakrishnan, Carol Handwerker, Hongwen Zhang, Babak Arfaei, Haley Fu, Qin Chen, Derek Daily, Ralph Lauwaert, Francis Mutuku, Kei Murayama, Murali Sarangapani, Daniel Werkhoven, "Interim Thermal Cycling Report on Hybrid and Homogeneous LTS Solder Joints," *Proceedings of SMTAI 2021*, 400-425, Minneapolis, MN, November 2021.
[38] Gregory Henshall, Keith Sweatman, Keith Howell, Joe Smetana and Richard Coyle, Richard Parker, Stephen Tisdale, Fay Hua, Weiping Liu, Robert Healey, Ranjit S. Pandher, Derek Daily, Mark Currie, Jennifer Nguyen, "iNEMI Lead-Free Alloy Alternatives Project Report: Thermal Fatigue Experiments and Alloy Test Requirements," *Proceedings of SMTAI*, 317-324, San Diego CA, 2009.
[39] Amkor Technology Datasheets: CABGA DS550T (Rev. 11/15) and CTBGA DSS550N (Rev. 1/07), Amkor Technology, www.amkor.com, Tempe, AZ.
[40] R. Aspandiar, N. Badwe, K. Byrd, K.K. Tang, L. Campbell and S. Mokler, "Investigation of Low Temperature Solders to Reduce Reflow Temperature, Improve SMT Yields and Realize Energy Savings," *Proceedings of the 2015 APEX Conference*, San Diego, CA, S14-03, February 2015.
[41] Richard Coyle, Dave Hillman, Richard Parker, Charmaine Johnson, Michael Osterman, Jasbir Bath, Babak Arfaei, Andre Delhaise, Keith Howell, Brook Sandy-Smith, Joe Smetana, Stuart Longgood, "The Effect of Bismuth, Antimony, or Indium on the Thermal Fatigue of High Reliability Pb-Free Solder Alloys," *Proceedings of SMTAI*, Rosemont, IL, October 2018.
[42] Richard Coyle, Dave Hillman, Charmaine Johnson, Richard Parker, Brook Sandy-Smith, Hongwen Zhang, Jie Geng, Michael Osterman, Babak Arfaei, Andre Delhaise, Keith Howell, Jasbir Bath, Joe Smetana, Stuart Longgood, Andre Kleyner, Julie Silk, Ranjit Pandher, Eric Lundeen, and Jerome Noiray "Alloy Composition and Thermal Fatigue of High Reliability Pb-Free Solder Alloys," *Proceedings of SMTAI*, Rosemont, IL, October 2018.
[43] Richard Coyle, Charmaine Johnson, Dave Hillman, Richard Parker, Michael Osterman, Joe Smetana, Tim Pearson, Babak Arfaei, Keith Howell, Stuart Longgood, Andre Kleyner, Julie Silk, Andre Delhaise, Hongwen Zhang, Jie Geng, Ranjit Pandher, Eric Lundeen, "Thermal Cycling Reliability and Failure Mode of Two Ball Grid Array Packages with High Reliability Pb-Free Solder Alloys," *Proceedings of SMTA International*, 436-456, September 22-26, 2019, Rosemont, IL.
[44] IPC-9701B, "Thermal Cycling Test Method for Fatigue Life Characterization of Surface Mount Attachments," IPC, Bannockburn, IL, 2021.
[45] W.D. McCallister, Materials Science and Engineering: An Introduction, John Wiley & Sons, 2003, Chap 7.
[46] L. Coffin, Jr., Met. Eng. Q., Vol 3, p. 15 (1963).
[47] S. Manson, Thermal Stress and Low-Cycle Fatigue, McGraw-Hill, New York (1966).
[48] K.C. Norris and A. H. Landzberg, "Reliability of Controlled Collapse Interconnections," IBM J. Res. Dev., Vol. 13, No. 3, pp. 266-271 (1969).
[49] W. Engelmaier, "Fatigue Life of Leadless Chip Carrier Solder Joints During Power Cycling", IEEE Transactions on Components, Hybrids, and Manufacturing Technology, vol.6, no.3, pp. 232-237, September 1983
[50] F. Hadian, M. Genanu, R. Owen, and E. J. Cotts, "The dependence of the microstructure of SnAgCu/SnBiAg mixed assemblies on reflow temperature," in Proceedings of SMTA International, 2020, pp. 326–332.
[51] M. Genanu, F. Hadian, R. Owen, and E. J. Cotts, "The effect of thermal history on the microstructure of SnAgCu/SnBiAg mixed assemblies," J. Electron. Mater., no. In Press, 2020, doi: https://doi.org/10.1007/s11664-020-08474-3.
[52] "ImageJ: Image Processing and Analysis in Java," https://imagej.nih.gov/ij/index.html
[53] S. A. Belyakov J. Xian, G. Zeng, K. Sweatman, T. Nishimura, T. Akaiwa, C. M. Gourlay., "Precipitation and coarsening of bismuth plates in Sn–Ag–Cu–Bi and Sn–Cu–Ni–Bi solder joints," J. Mater. Sci. Mater. Electron., vol. 30,
[54] S. Dunford, S. Canumalla, and P. Viswanadham, "Intermetallic Morphology and Damage Evolution Under Thermomechanical Fatigue of Lead (Pb)-Free Solder Interconnections," *Proceedings of Electronic Components Technology Conference,* 726-736, Las Vegas, NV, June 1-4, 2004.
[55] Liang Yin, Luke Wentlent, Linlin Yang, Babak Arfaei, Awni Oasaimeh, and Peter Bargemen, "Recrystallization and Precipitate Coarsening in Pb-Free Solder Joints During Thermomechanical Fatigue," J. Electronic Materials, Vol. 41, No. 2, 241-252, 2011.
[56] Babak Arfaei, Francis Mutuku, Richard Coyle, Eric Cotts, and Jim Wilcox, "Failure Mechanism and Microstructural Evolution of Pb-free Solder Alloys in Thermal Cycling Tests: Effect of Solder Composition and Sn

Grain Morphology," *Proceedings 65th Electronic Components and Technology Conference*, 118-126, 2015.
[57] André Delhaise, "Solid-State Diffusion of Bismuth in Tin-Rich , Lead-Free Solder Alloys," A thesis submitted in conformity with the requirements for the degree of Doctor of Philosophy, Department of Materials Science & Engineering University of Toronto, 67, 2018
[58] David A. Porter, Kenneth E. Easterling, and Mohammed Y. Sherif, **Phase Transformations in Metals and Alloys**, Third Edition, 112, CRC Press Taylor, 2009.
[59] J. W. Morris, Jr, J. L. Freer Goldstein, and Z. Mei, ‘‘Microstructural Influences on the Mechanical Properties of Solder’’, in **The Mechanics of Solder Alloy Interconnects**, edited by D. Frear, H. Morgan, S. Burchett, and J. Lau, Van Nostrand Reinhold, New York, 1994.
[60] L. Wentlent, J. Wilcox, and M. Meilunas, "Reliability Behavior of Surface Mount Devices Assembled with Bismuth Bearing Low-Melt Solder Pastes," *Proceedings of SMTAI Virtual,* 442-450, September 28- October 23, 2020.
[61] Richard Coyle, Faramarz Hadian, Raiyo Aspandiar, Vasu Vasudevan, Aileen Allen, Morgana Ribas, Keith Howell, Jagadeesh Radhakrishnan, Dan Burkholder, Pubudu Goonetilleke, Hongwen Zhang, Carol Handwerker, Babak Arfaei, Qin Chen, Derek Daily, Ralph Lauwaert, Francis Mutuku, Huaguang Wang, Haley Fu, Kei Murayama, Murali Sarangapani, and Daniel Werkhoven, "Thermal Cycling Performance of Hybrid, Homogeneous, and Resin Reinforced Low Temperature Solder Ball Grid Array Interconnects," *Proceedings of SMTA International 2022*, 461-492, Minneapolis, MN, October 31 – November 3, 2022.
[62] Dan Burkholder, Russ Brown, Raiyo Aspandiar, Jagadeesh Radhakrishnan, Pubudu Goonetilleke, Yunfei Wang, Richard Coyle, Faramarz Hadian, Babak Arfaei, Vasu Vasudevan, Aileen Allen, Keith Howell, Qin Chen, Derek Daily, Haley Fu, Carol Handwerker, Ralph Lauwaert, Daniel Werkhoven, Kei Murayama, Hongwen Zhang, Francis Mutuku, Huaguang Wang, Morgana Ribas, and Murali Sarangapani, "The Effect of Thermal Cycling Profile on Thermal Fatigue Performance of a 192-Pin Chip Array BGA with Hybrid, Homogeneous, and Resin Reinforced Low Temperature Solder Interconnects," *Proceedings of SMTA International 2022*, 493-528, Minneapolis, MN, October 31 – November 3, 2022.

APPENDIX A

Experimental Test Vehicle – Component and Test Board Information

BGA Package Attributes		
Designation	CABGA192	CTBGA84
Die Size	12x12 mm	5x5 mm
Package Size	14x14 mm	7x7 mm
Ball Array	16x16	12x12
Ball Pitch	0.8 mm	0.5 mm
Ball Diameter	0.46 mm	0.3 mm
Pad Diameter	0.381 mm	0.3 mm
Pad Finish	Electrolytic Ni/Au	Electrolytic Ni/Au
Au thickness	0.6 µm	0.6 µm
PCB Attributes		
Dimensions	165 x 178 x 2.36 mm	
Laminate	Shengyi S7545	
Surface Finish	ENTEK Plus HT (OSP)	
No. Cu Layers	6	
Pad Diameter	0.356 mm	0.254 mm
Solder Mask Dia.	0.483 mm	0.381 mm
Glass Transition Temperature, T_g	146 °C (DSC) 168 °C (TMA)	
Decomposition Temperature, T_d	374 °C	

Table A-1. BGA package and PCB attributes [37].

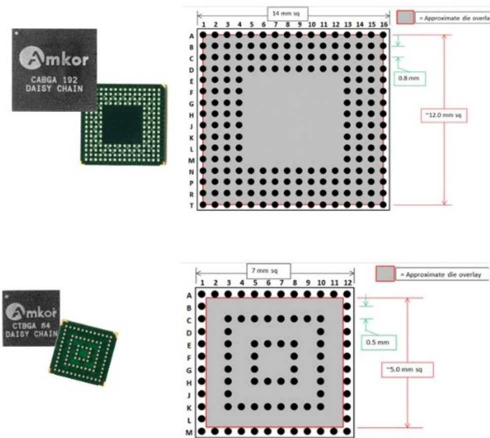

Figure A-1. The CABGA192 and CTBGA84 daisy chained components and pin diagrams with die sizes and locations [37, 39].

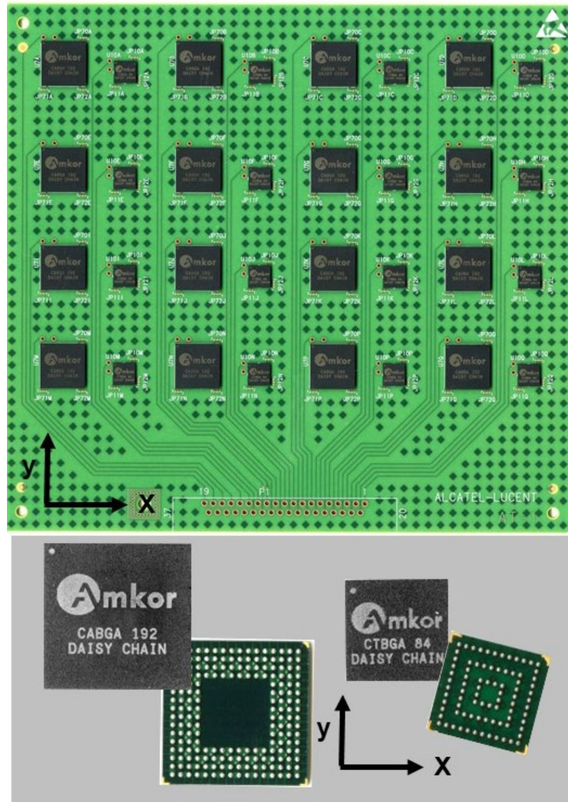

Figure A-2. A fully populated, daisy chained PCB and the daisy chained CABGA192 and CTBGA84 components [37].

APPENDIX B

Board Assembly Parameters – Experimental Design

Leg #	Leg Name	Component	Component Sphere Composition	Solder Paste Alloy	Solder Paste Category
1	SAC Baseline	CTBGA84 CABGA192	SAC305	SAC305	SAC Baseline
2	Beserah JRP	CTBGA84 CABGA192	SAC305	BiSn Eutectic	Joint Reinforced Paste (JRP)
3	Golden Pillow 2 JRP	CTBGA84 CABGA192	SAC305	BiSn + Microalloys	Joint Reinforced Paste (JRP)
4	Heterogeneous Red Flesh	CTBGA84 CABGA192	SAC305	BiSn + Microalloys	Ductile BiSn
5	Heterogeneous Sultan 2	CTBGA84 CABGA192	SAC305	BiSn + Microalloys	Ductile BiSn
6	Homogeneous Red Flesh	CTBGA84 CABGA192	Identical to Solder Paste	BiSn + Microalloys	Ductile BiSn
7	Homogeneous Sultan 2	CTBGA84 CABGA192	Identical to Solder Paste	BiSn + Microalloys	Ductile BiSn

Table B-1. The 7 Experimental Legs for the Temperature Cycling Tests [37].

APPENDIX C

Board Assembly Parameters – Stencil Design and Printed Solder Paste Volume

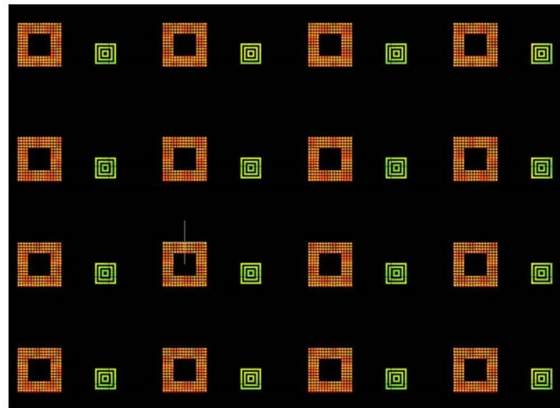

Package	Description above	Dimension		Geometry	Paste-to-Ball Volume Ratio
CABGA192	(orange)	0.53 mm	21 mils	Square	0.57
CTBGA84	(green)	0.28 mm	11 mils	Square	0.56

Figure C-1: Stencil aperture designs for the two components on the Alloy ATC TV board [37].

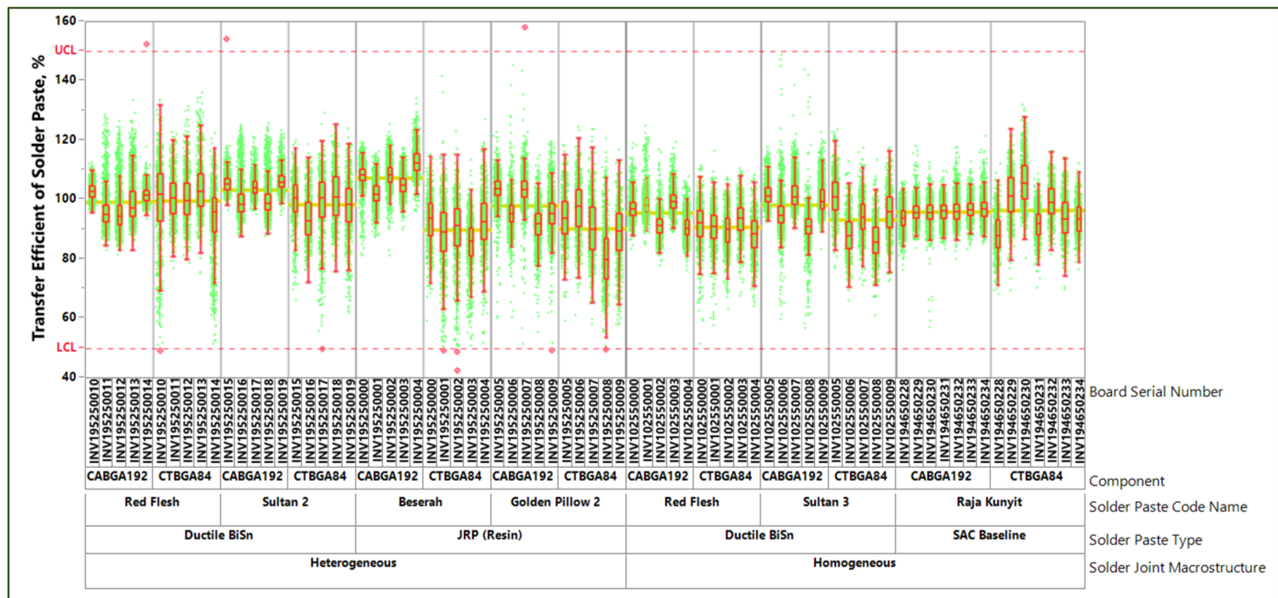

Figure C-2: Solder Paste Transfer Efficiency for the Solder Pastes used in this study to assemble the Alloy ATC TV board [37, 61, 62].

APPENDIX D

Board Assembly Parameters – Reflow Soldering Profiles

Code Name	Raja Kunyit	Red Flesh	Sultan 2	Beserah	Golden Pillow 2
Solder Paste Type	SAC	Ductile BiSn		JRP (Resin)	
Wt.% Bi	0	40	56-58	58	58
Wt.% Ag	3	0	<1	0	0
Initial Melting Temp, °C	217	139	138	139	140
Liquidus Temp, °C	220	179	145	139	140

Table D-1. Wt.% Bi, Wt.% Ag, Initial Melting and Liquidus Temperatures of the five solder pastes used in this study [37].

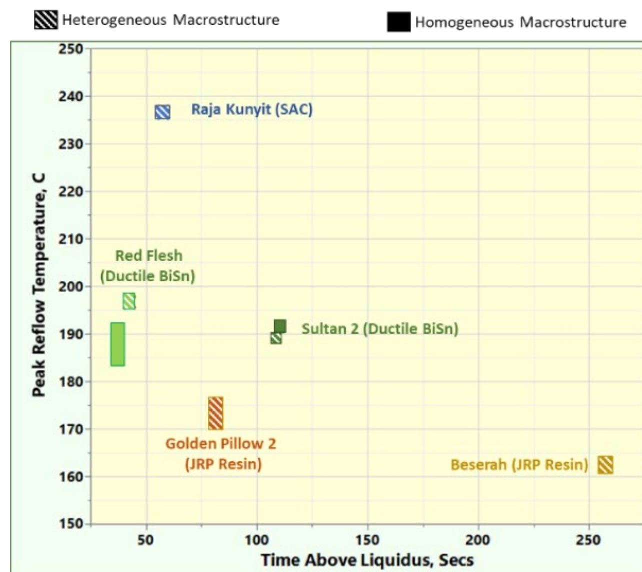

Figure D-1. The Peak Reflow Temperature (C) and Time Above Liquidus (seconds) for the alloys used in this study [37].

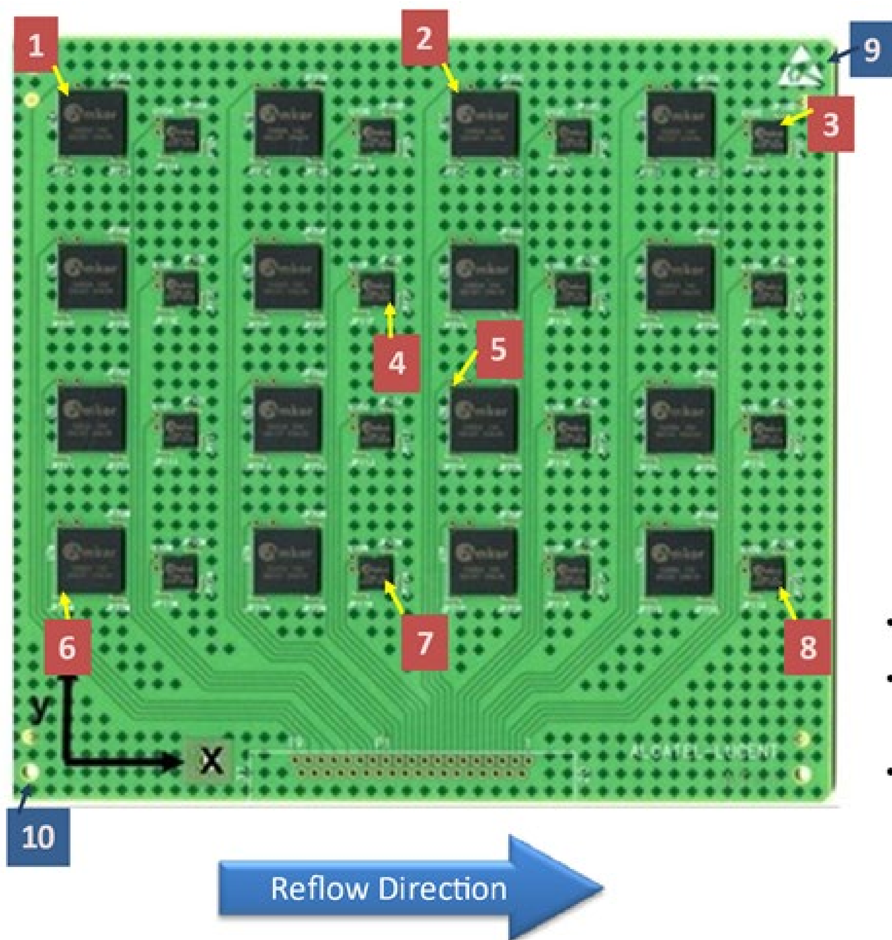

Ref. Des. (Pin Location shown at left)

TC1: U7A
TC2: U7C
TC3: U10D
TC4: U10F
TC5: U7K
TC6: U7M
TC7: U10N
TC8: U10Q
TC9: Board Surface upper right corner
TC10: Board Surface lower left corner

- Drill PCB to attach TC#s 1-8.
- TC#9 and TC#10 can be epoxied to top of board.
- General location is shown on the board photo with an arrow. Exact pin is not required.

Figure D-2. The location of the thermocouples on the Alloy ATC TV board for measurement the Reflow Profiles of various experimental legs [37, 61, 62].

Oven Name: BTU01 | Process Window Name: INEMI ATC ALLOY TV_PS_64800-05

Setpoints (Degree Celsius)												
Zone	1	2	3	4	5	6	7	8	9	10	11	12
Top	150	155	170	175	180	180	185	210	230	265	265	230
Bottom	150	155	170	175	180	180	185	210	230	265	265	230
Conveyor Speed (cm/min):	92.0											

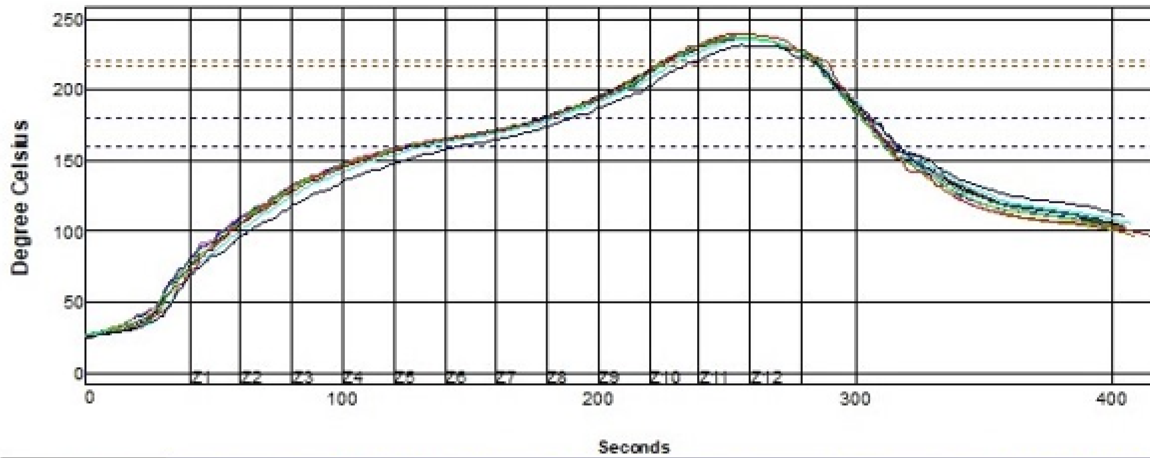

PWI = 202%	Max Rising Slope		Max Falling Slope		Soak Time 160-180°C		Peak Temp		Tot Time /217°C		Tot Time /220°C-2	
TC1	1.86	24%	-2.06	57%	55.48	40%	237.67	-49%	64.08	154%	59.87	98%
TC2	1.87	25%	-2.04	59%	53.07	8%	236.90	-54%	63.75	150%	59.23	90%
TC3	1.83	22%	-2.07	57%	54.68	29%	237.34	-51%	63.51	147%	59.32	91%
TC4	1.94	29%	-1.93	63%	52.76	4%	237.06	-53%	63.43	146%	59.28	90%
TC5	1.89	26%	-1.88	65%	52.67	2%	236.12	-59%	62.62	135%	58.21	76%
TC6	1.91	28%	-1.92	63%	54.62	28%	237.01	-53%	60.83	111%	56.37	52%
TC7	1.91	27%	-1.91	63%	50.40	-28%	235.45	-64%	60.27	104%	55.72	43%
TC8	1.96	31%	-2.06	58%	53.84	18%	237.28	-51%	63.27	144%	59.37	92%
TC9	1.95	30%	-2.27	49%	52.36	-2%	240.01	-33%	67.62	202%	64.26	157%
TC10	1.76	17%	-1.80	68%	43.59	-119%	231.23	-92%	52.33	-2%	44.72	-104%
Delta	0.20		0.47		11.89		8.78		15.29		19.54	

Figure D-3. Reflow Profile for the Raja Kunyit paste used in Leg #1, the SAC Baseline category [37, 61, 62].

Oven Name: BTU02 **Process Window Name: INEMI ATC ALLOY TV_PS_64800-05_LEG2**

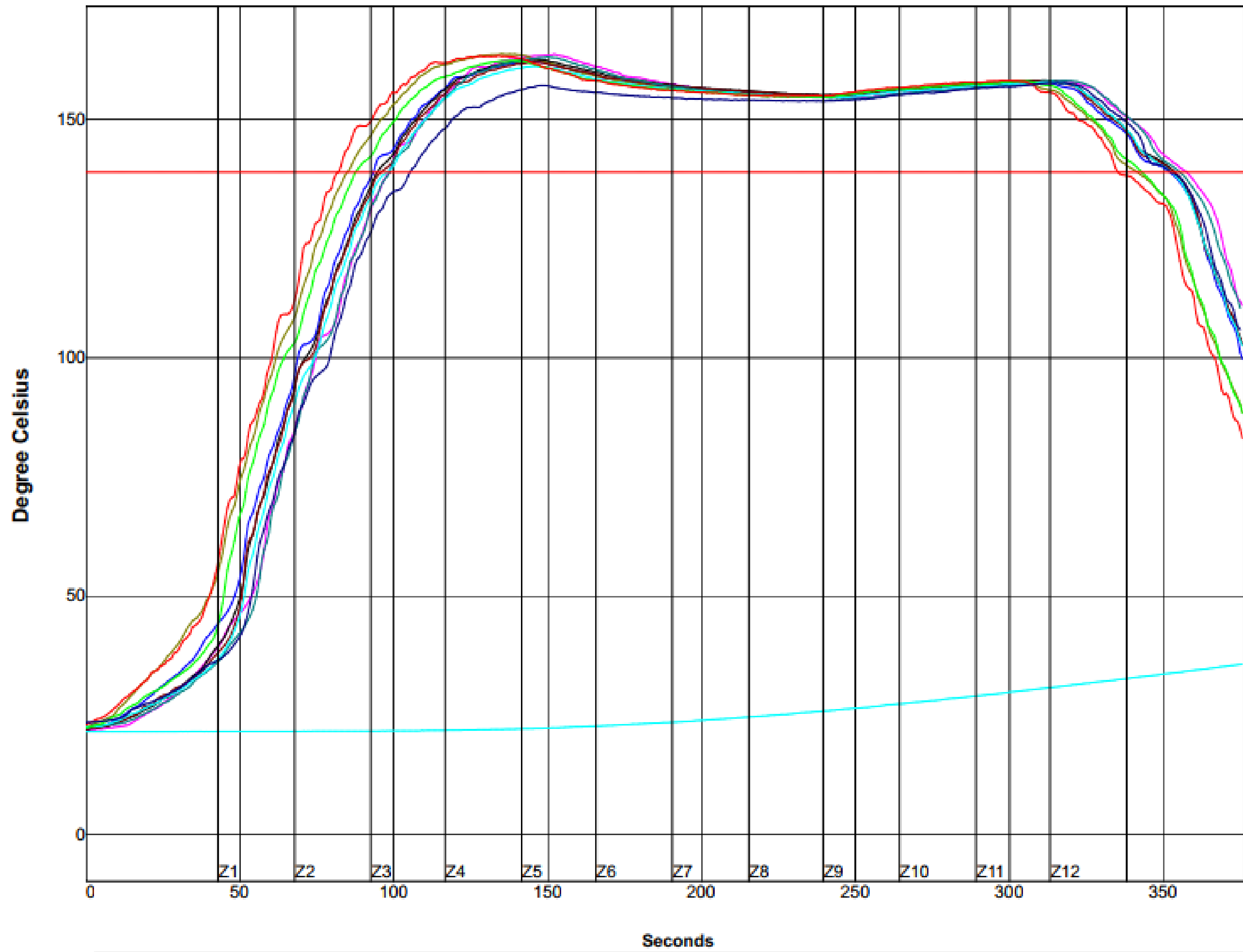

PWI= 88%	Max Rising Slope		Reflow Time /139°C		Peak Temp	
TC1	2.14	12%	258.95	-68%	163.73	75%
TC2	2.11	9%	258.44	-69%	162.23	45%
TC3	2.12	10%	256.60	-72%	163.78	76%
TC4	2.15	12%	259.08	-68%	162.73	55%
TC5	2.20	16%	257.53	-71%	162.12	42%
TC6	2.22	19%	256.60	-72%	163.17	63%
TC7	2.16	13%	254.92	-75%	161.23	25%
TC8	2.28	23%	255.42	-74%	162.45	49%
TC9	2.27	23%	253.26	-78%	163.45	69%
TC10	2.10	8%	247.14	-88%	157.78	-44%
Delta	0.18		11.94		6.00	

Figure D-4. Reflow Profile for the Beserah paste used in Leg #2, the JRP Resin category [37, 61, 62].

Oven Name: BTU02

Process Window Name: INEMI ATC ALLOY
TV_PS_64800-05_LEG3

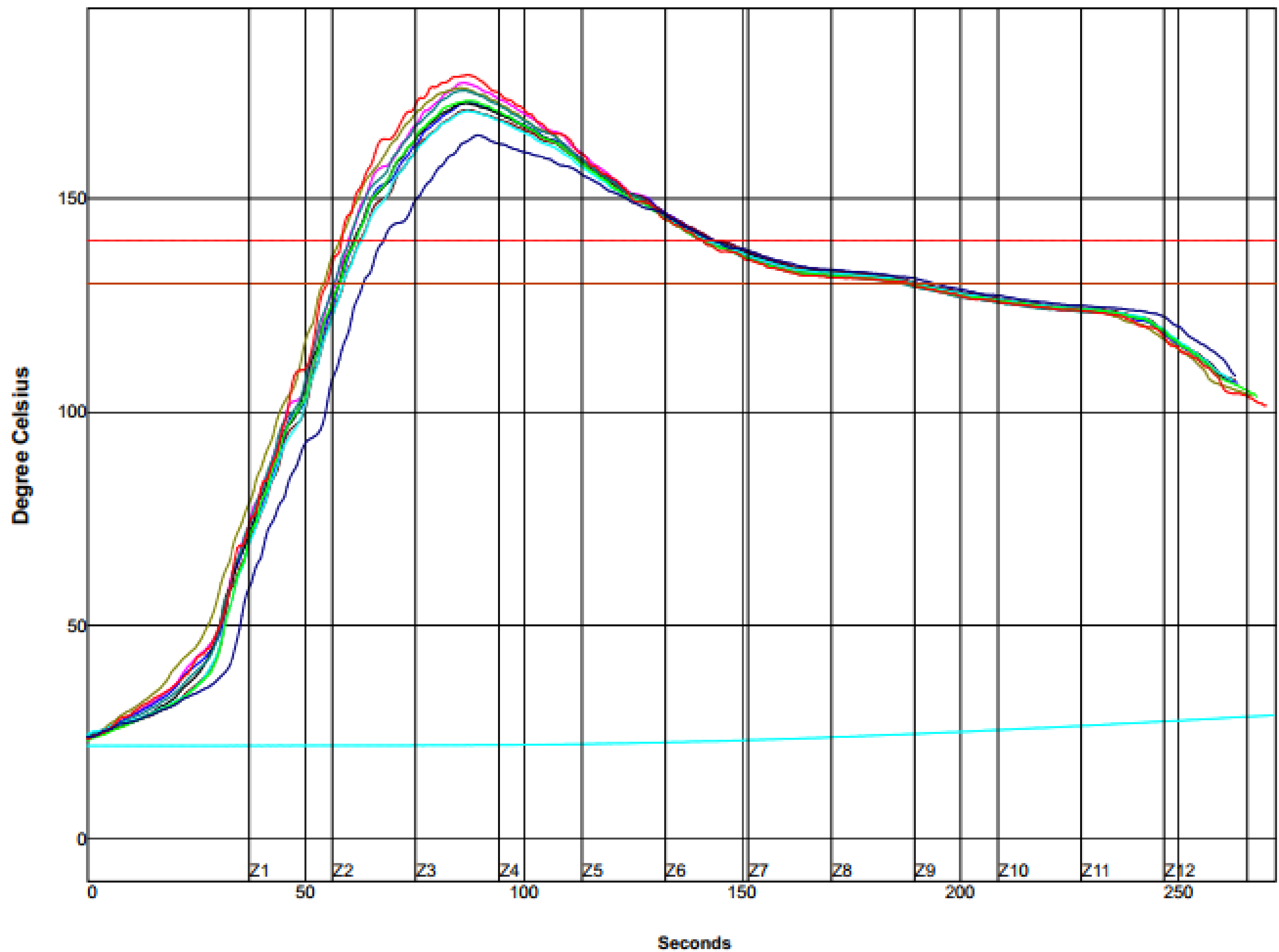

PWI= 168%	Max Rising Slope		Reflow Time /140°C		Peak Temp		Tot Time /130°C	
TC1	3.01	1%	82.89	129%	177.17	-4%	131.33	-87%
TC2	2.91	-9%	82.57	126%	172.67	-64%	133.38	-66%
TC3	2.90	-10%	83.51	135%	175.95	-21%	133.67	-63%
TC4	2.91	-9%	82.71	127%	172.45	-67%	132.77	-72%
TC5	2.93	-7%	82.52	125%	170.78	-90%	132.03	-80%
TC6	3.02	2%	81.18	112%	175.34	-29%	129.86	-101%
TC7	2.91	-9%	79.69	97%	170.56	-93%	131.04	-90%
TC8	3.04	4%	79.82	98%	172.95	-61%	130.83	-92%
TC9	3.12	12%	82.89	129%	179.01	20%	133.61	-64%
TC10	2.84	-16%	76.01	60%	164.90	-168%	130.73	-93%
Delta	0.28		7.50		14.11		3.81	

Figure D-5. Reflow Profile for the Golden Pillow 2 paste used in Leg #3, the JRP category [37, 61, 62].

Oven Name: BTU02 Process Window Name: INEMI ATC ALLOY TV_PS_64800-05_LEG4

Setpoints (Degree Celsius)												
Zone	1	2	3	4	5	6	7	8	9	10	11	12
Top	130	130	130	130	130	135	150	185	230	240	225	150
Bottom	130	130	130	130	130	135	150	185	230	240	225	150
Conveyor Speed (cm/min):	125.0											

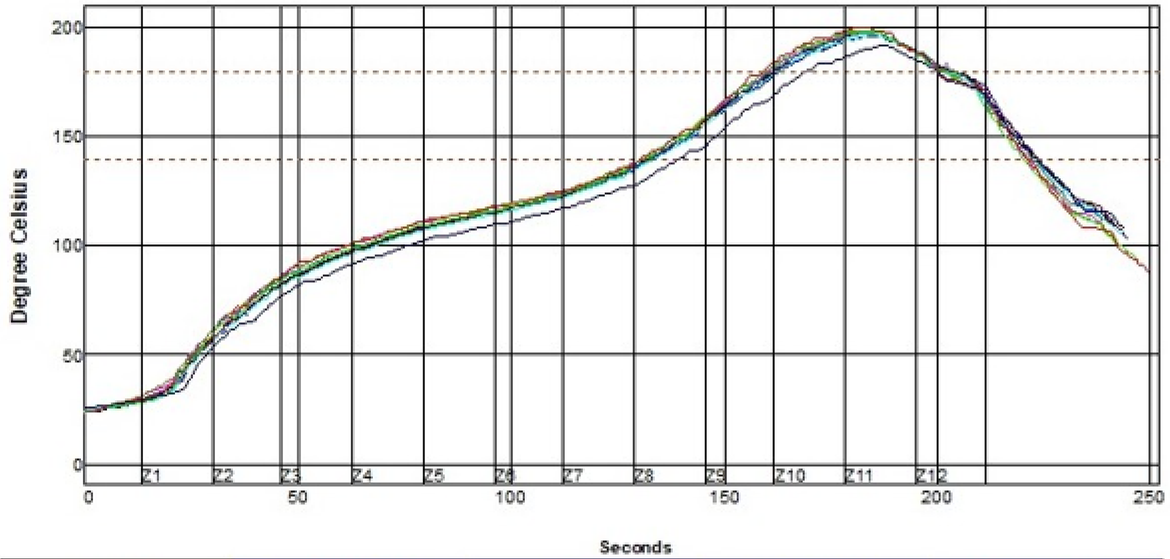

PWI= 106%	Max Rising Slope		Peak Temp		Tot Time /139°C		Tot Time /179°C-2	
TC1	1.68	-32%	197.73	55%	90.49	102%	44.55	-51%
TC2	1.63	-37%	195.51	10%	91.17	104%	40.95	-63%
TC3	1.65	-35%	198.28	66%	91.87	106%	42.45	-59%
TC4	1.65	-35%	197.28	46%	91.52	105%	43.56	-55%
TC5	1.65	-35%	196.06	21%	91.11	104%	42.82	-57%
TC6	1.66	-34%	197.56	51%	90.03	100%	43.51	-55%
TC7	1.66	-34%	196.28	26%	89.77	99%	40.55	-65%
TC8	1.72	-28%	197.78	56%	89.52	98%	42.66	-58%
TC9	1.76	-24%	199.56	91%	91.01	103%	41.22	-63%
TC10	1.53	-47%	191.45	-71%	84.22	81%	31.65	-94%
Delta	0.23		8.11		7.65		12.90	

Figure D-6. Reflow Profile for the Red Flesh paste used in Leg #4, the Hybrid (Heterogeneous) Ductile BiSn category [37, 61, 62].

Oven Name: BTU02 Process Window Name: INEMI ATC ALLOY TV_PS_64800-05_LEG5

Setpoints (Degree Celsius)												
Zone	1	2	3	4	5	6	7	8	9	10	11	12
Top	130	125	120	120	125	135	150	175	205	210	205	160
Bottom	130	125	120	120	125	135	150	175	205	210	205	160
Conveyor Speed (cm/min):	92.0											

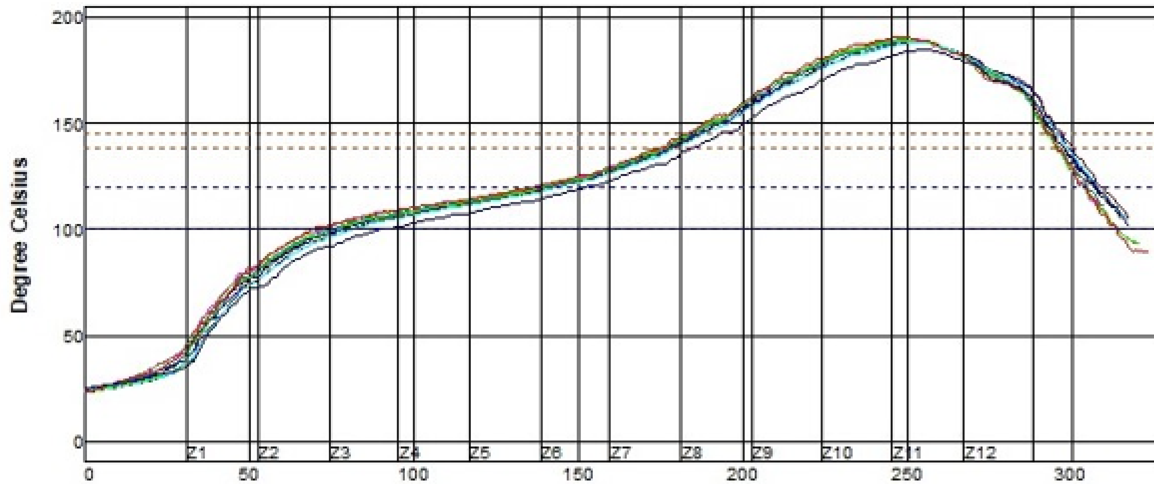

PWI= 118%	Max Rising Slope		Soak Time 100-120°C		Peak Temp		Tot Time /138°C		Tot Time /145°C-2	
TC1	1.54	2%	64.45	-70%	189.56	-30%	120.86	106%	109.51	30%
TC2	1.54	2%	62.19	-85%	188.12	-49%	122.00	113%	110.00	33%
TC3	1.53	2%	64.54	-70%	189.56	-30%	121.37	109%	109.77	32%
TC4	1.56	4%	62.41	-84%	189.28	-34%	122.63	118%	109.84	32%
TC5	1.58	5%	61.36	-91%	188.51	-44%	121.98	113%	109.80	32%
TC6	1.58	5%	64.88	-67%	189.45	-32%	119.61	97%	108.38	23%
TC7	1.57	5%	62.56	-83%	188.51	-44%	119.86	99%	107.62	17%
TC8	1.65	10%	63.00	-80%	189.23	-35%	120.41	103%	108.63	24%
TC9	1.60	6%	68.27	-45%	190.51	-19%	120.58	104%	110.96	40%
TC10	1.48	-5%	62.03	-86%	185.01	-87%	113.97	60%	101.84	-21%
Delta	0.17		6.91		5.50		8.66		9.12	

Figure D-7. Reflow Profile for the Sultan 2 paste used in Leg #5, the Hybrid (Heterogeneous) Ductile BiSn category [37, 61, 62].

Oven Name: BTU01

Process Window Name: INEMI ATC ALLOY TV_093_PS DP 5600 LMPA

Setpoints (Degree Celsius)												
Zone	1	2	3	4	5	6	7	8	9	10	11	12
Top	130	130	130	130	130	135	150	180	230	230	220	150
Bottom	130	130	130	130	130	135	150	180	230	230	220	150
Conveyor Speed (cm/min):	125.0											

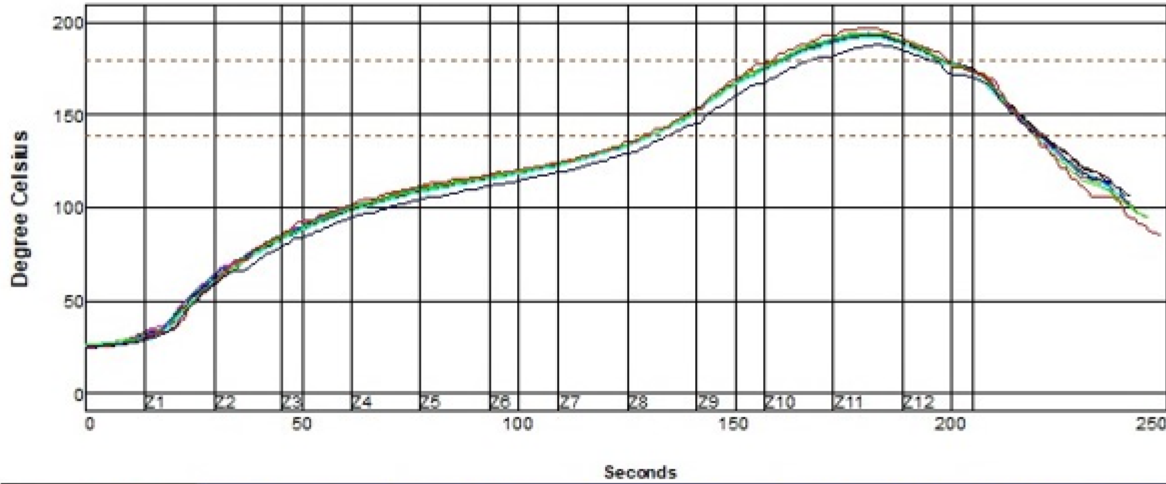

PWI= 145%	Max Rising Slope		Max Falling Slope		Peak Temp		Tot Time /139°C		Tot Time /179°C-2	
TC1	1.62	-38%	-1.95	37%	192.90	-42%	89.10	97%	38.02	-73%
TC2	1.64	-36%	-2.02	32%	192.56	-49%	89.82	99%	37.25	-76%
TC3	1.65	-35%	-2.08	28%	194.23	-15%	90.60	102%	38.80	-71%
TC4	1.68	-32%	-1.91	39%	193.34	-33%	91.11	104%	38.52	-72%
TC5	1.65	-35%	-1.90	40%	192.06	-59%	90.28	101%	36.87	-77%
TC6	1.67	-33%	-1.91	39%	193.90	-22%	89.48	98%	39.09	-70%
TC7	1.66	-34%	-1.91	39%	191.78	-64%	88.90	96%	35.49	-82%
TC8	1.71	-29%	-2.05	30%	194.28	-14%	89.10	97%	38.19	-73%
TC9	1.78	-22%	-2.26	16%	196.84	37%	90.72	102%	40.65	-65%
TC10	1.57	-43%	-1.82	45%	187.73	-145%	85.36	85%	28.79	-104%
Delta	0.21		0.44		9.11		5.75		11.86	

Figure D-8. Reflow Profile for the Red Flesh paste used in Leg #6, the Homogeneous Ductile BiSn category [37, 61, 62].

Oven Name: BTU01

Process Window Name: INEMI ATC ALLOY TV_093_PS DP 5600 LMPA

Setpoints (Degree Celsius)												
Zone	1	2	3	4	5	6	7	8	9	10	11	12
Top	135	130	125	120	122	135	155	190	210	210	210	170
Bottom	135	130	125	120	122	135	155	190	210	210	210	170
Conveyor Speed (cm/min):	98.0											

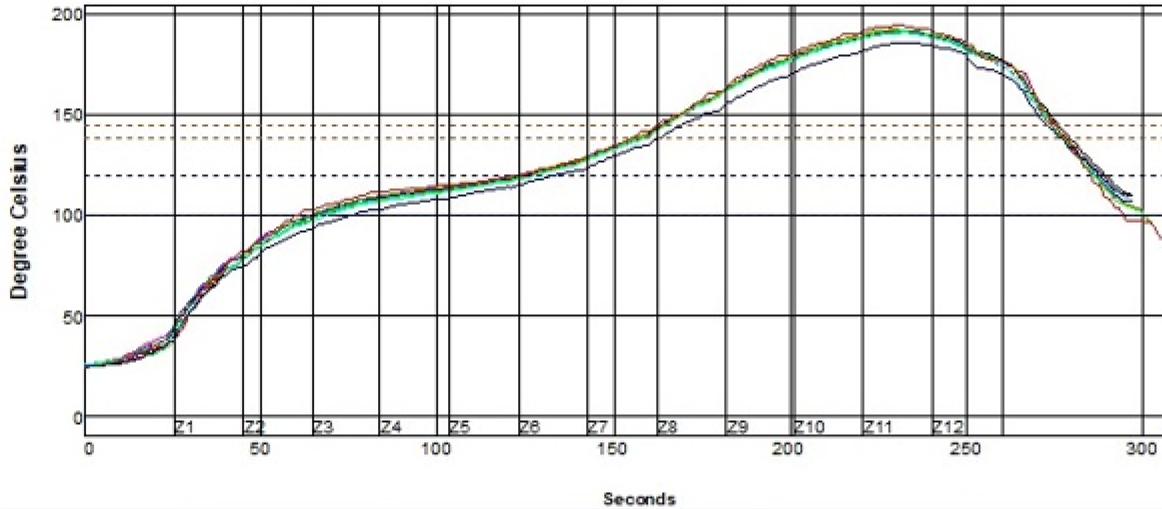

PWI= 138%	Max Rising Slope		Preheat 100-120°C		Peak Temp		Tot Time /138°C		Tot Time /145°C-2	
TC1	1.58	-42%	60.59	-96%	191.28	26%	119.12	91%	111.38	14%
TC2	1.63	-37%	59.72	-102%	191.73	35%	122.08	121%	111.87	19%
TC3	1.64	-36%	59.54	-103%	192.40	48%	123.58	136%	111.26	13%
TC4	1.66	-34%	59.31	-105%	191.95	39%	122.86	129%	111.48	15%
TC5	1.62	-38%	58.57	-110%	190.95	19%	121.25	113%	111.21	12%
TC6	1.64	-36%	61.94	-87%	190.73	15%	118.77	88%	109.17	-8%
TC7	1.65	-35%	58.91	-107%	190.51	10%	119.43	94%	109.85	-1%
TC8	1.71	-29%	59.72	-102%	192.06	41%	121.36	114%	109.69	-3%
TC9	1.77	-23%	63.94	-74%	194.40	88%	123.79	138%	111.63	16%
TC10	1.55	-45%	58.27	-112%	185.84	-83%	114.87	49%	102.97	-70%
Delta	0.22		5.67		8.56		8.92		8.90	

Figure D-9. Reflow Profile for the Sultan 2 paste used in Leg #7, the Homogeneous Ductile BiSn category [37, 61, 62].

APPENDIX E

Board Assembly Parameters – Post Reflow Soldering Daisy Chain Resistances

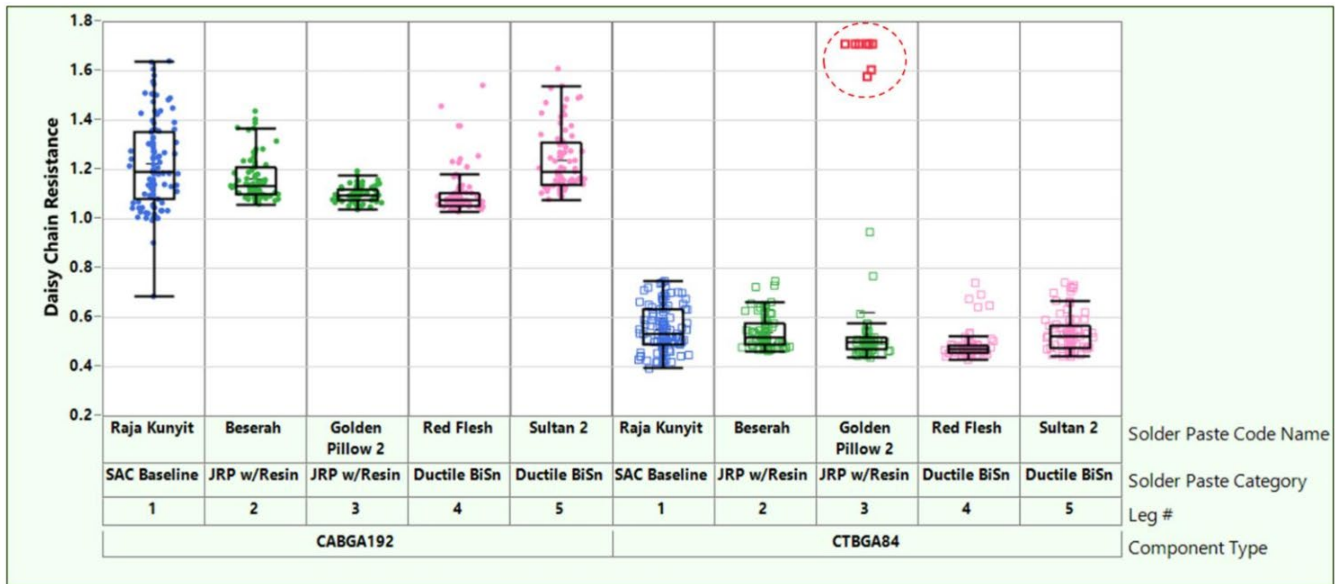

Figure E-1. Resistances of the Daisy Chains for the two Component Types on the Alloy ATC TV Boards after reflow soldering for all Legs in this Study [37, 61, 62].